

~~Building up a subsurface geological model in active offshore areas: constraints from legacy seismic reflection profiles and deep wells in the 2022 Fano-Pesaro Mw 5.5 earthquake sequence area (Adriatic Sea, Italy).~~

5 New geological constraints on the subsurface structure of the 2022 Fano-Pesaro Mw 5.5 earthquake sequence area (Adriatic Sea, Italy) from legacy seismic reflection images and deep well information.

Elham Safarzadeh¹, Maurizio Ercoli^{1,3}, Filippo Carboni^{2,3}, Francesco Mirabella¹, Assel Akimbekova⁴, Massimiliano R. Barchi¹

10 ¹ Department of Physics and Geology, University of Perugia, Italy

² Institute of Earth and Environmental Sciences (Geology), Albert-Ludwigs-University Freiburg, Germany

³ CRUST Member (Centro interUniversitario per l'analisi SismoTettonica Tridimensionale Con Applicazioni Territoriali), Italy

⁴ Eni Exploration and Production Division, Via Emilia, 1, 20097 San Donato Milanese, Milan, Italy

Correspondence to: Safarzadeh, E (elham.safarzadeh@dottarandi.unip.it)

15

Abstract

~~Building~~ Studying the a subsurface geological model in offshore areas is a complex task, ~~due to the inaccessibility of outcrops and the resulting inaccessibility~~ obvious absence of outcrops and thus the inaccessibility to of the study site ~~as it is impossible or very challenging directly accessing any eventual outcrops at the study site.~~ The integration of key seismic reflection and borehole data is therefore fundamental, even if only available as legacy data on paper hard copy and/or characterized by an apparent low quality. However, such data are often the only ones available, and can still provide a high amount of detailed information for building a reliable geological model ~~which can be to be compared with and discussed with about the~~ seismicity distribution in active areas. In this work, legacy seismic reflection profiles calibrated with boreholes, are used to propose a new geological model of the frontal part of the Northern Apennines area struck by the 2022 Fano-Pesaro Mw 5.5 earthquake sequence (Adriatic Sea, Italy). ~~The legacy seismic data were digitized and converted to SEG-Y format, and some basic post-processing stack filterings were applied to enhance data quality.~~ The observed tectonic structures ~~are originated~~ originate from by multiple décollements located at different depths and show a strong relationship between the faulting depth and the ~~anticlines~~ wavelength of the anticlines. Two structures, namely the Pesaro and the Cornelia anticlines, are interpreted as ~~being~~ related to deep-seated thrusts, showing an en-echelon arrangement and thin-skinned deformation. A

20

25

30 smaller wavelength structure, namely the Tamara antiform, is interpreted to be ~~related to~~associated with shallow-seated imbricated fore-verging thrusts in the forelimb of the Pesaro anticline. We highlight the importance of constructing a well-constrained geological model by integrating legacy geological and geophysical data, aimed at studying both offshore seismotectonic ~~settings studies settings. as well as at supporting industrial applications, particularly in the context of energy transition.~~

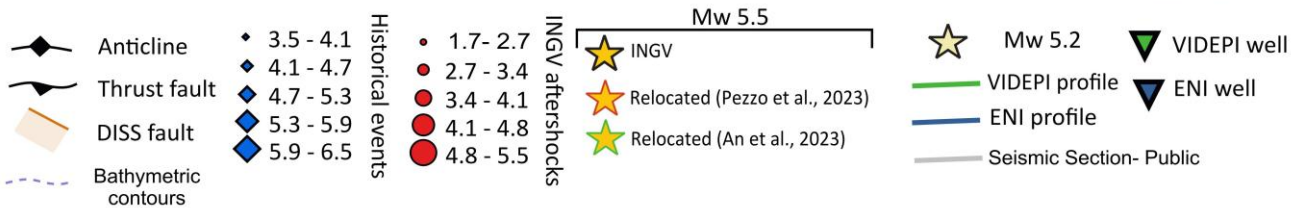
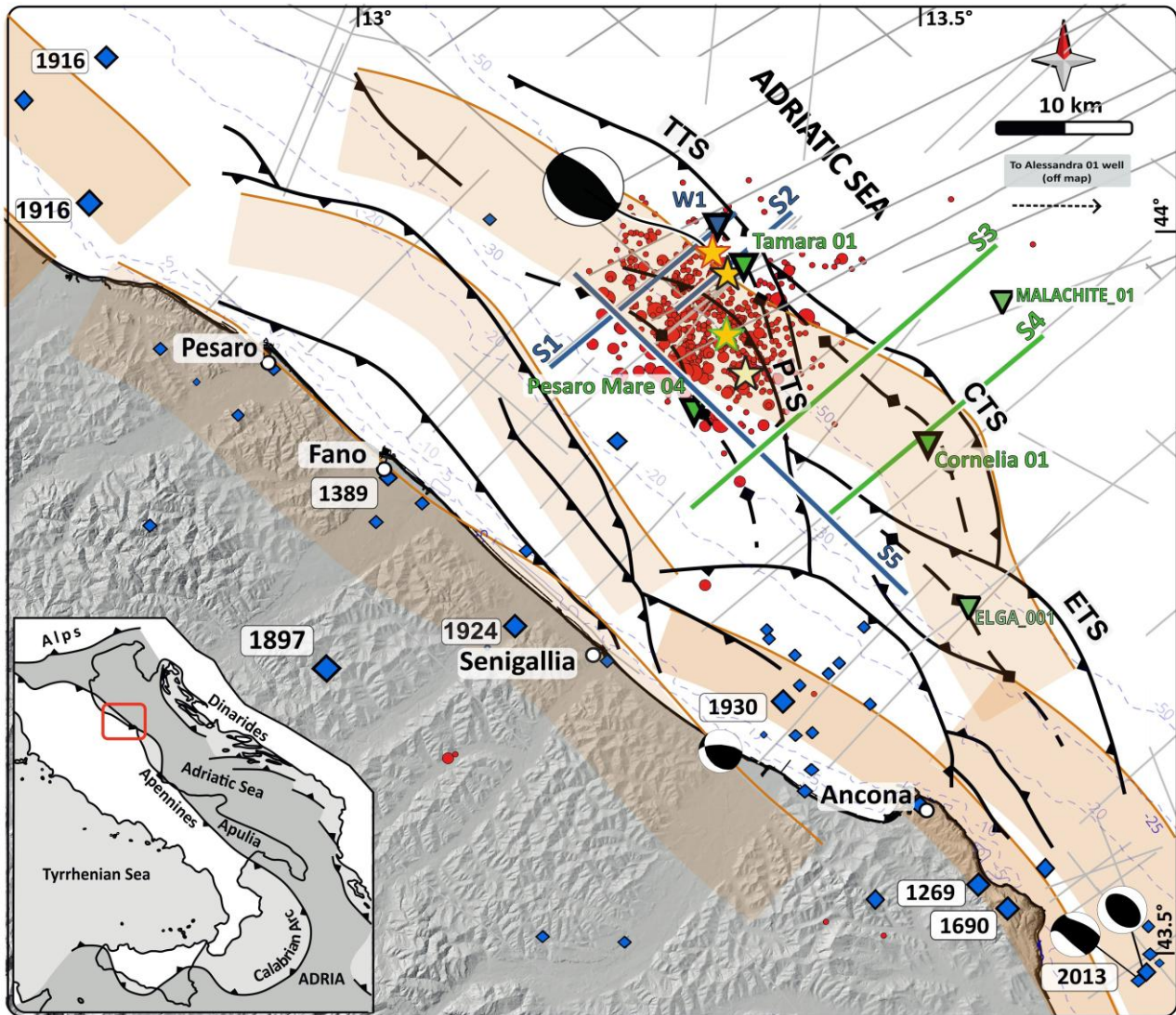
35 1. Introduction

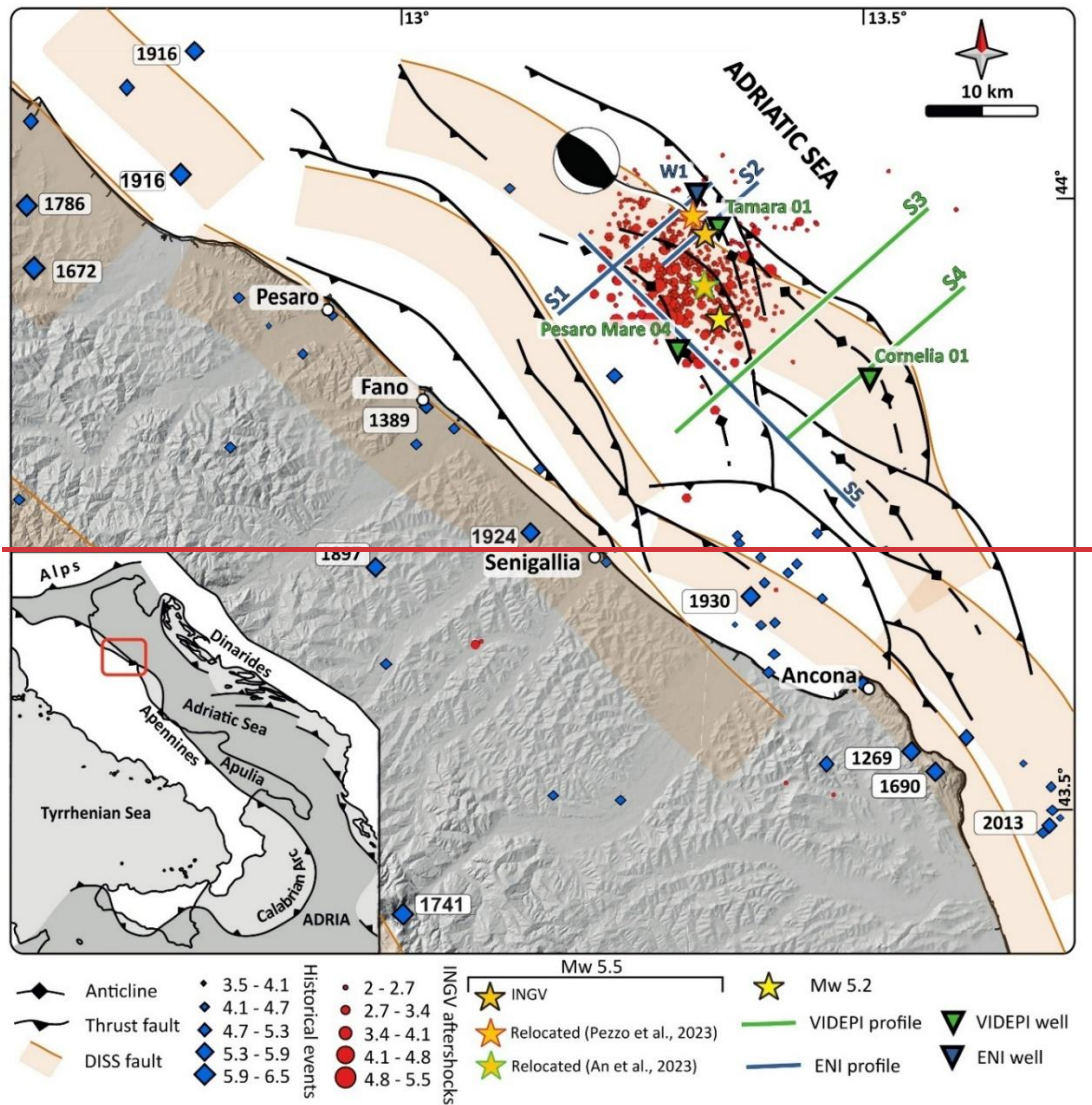
Buried and blind thrust faults, particularly those beneath the seafloor, pose considerable ~~difficulties~~challenges for ~~the study of global seismic activity~~determining their seismic potential and understanding the association between seismic activity and geological structures (Berberian, 1995; Roering et al., 1997; Gunderson et al., 2013; Panara et al., 2021). Despite their hidden nature, they ~~are capable~~pose substantial natural hazard ~~being capable to produce~~of producing strong earthquakes (\geq Mw 6.0: United States Geological Survey, n.d.) and ~~related triggering~~ underwater landslides and tsunamis (Lettis et al., 1997; Ioualalen et al., 2017; Takashimizu et al., 2020; Maramai et al., 2022). As coastal populations and infrastructure continue to expand, ~~the~~ understanding ~~of~~ the behaviour of these offshore buried faults becomes essential for mitigating both seismic and tsunami risks. Their detection is especially challenging, as it heavily relies on indirect observations such as geophysical data (Roering et al., 1997; Déverchère et al., 2005; Hayes et al., 2010; Sorlien et al., 2013; Franklin et al., 2019). Seismic reflection is one of the ~~best~~most effective geophysical tools able to provide high-resolution detailed images of the subsurface, ~~being capable of~~ illuminating depths where the upper crust earthquakes are located. These data are suitable ~~to for identify~~identifying the faults ~~faults'~~ geometry, kinematics, hierarchy and dynamics as well as the overall subsurface geological setting and the position of ~~the different lithologic~~ies ~~bodies which posses different velocity of seismic waves propagation~~units (e.g. Barchi et al., 2021). The Adriatic Sea in central Italy (Fig. 1) is a clear challenging example in terms of risk assessment, as the nearby coastlines are densely populated and many critical infrastructures have been developed during over the last ~~tens of years~~decades. In this region, the buried and blind thrust faults, ~~present in the offshore area~~located offshore, play a key role in the regional seismotectonic setting, but their detection is particularly challenging due to the high sedimentation rate of the area (Ricci Lucchi, 1986; Frignani and Langone, 1991; Barbieri et al., 2007; Ghielmi et al., 2013; Amadori et al., 2020) and the generally low-quality of the available geophysical data, ~~frequently being~~which are often legacy seismic reflection profiles.

55 While the axial zone of the Northern Apennines, located about 70 km onshore to the Westwest, is affected by extensional seismicity (Lavecchia et al., 1994; Ciaccio et al., 2005; Chiaraluce et al., 2017; Porreca et al., 2018; Barchi et al., 2021; Suga et al., 2023), the seismic events recorded in the offshore Marche region (Central Italy, along the Adriatic Sea coast) are mainly compressive, ~~and are~~ caused by buried active thrusts faults (Argnani, 1998; Maesano et al., 2013; Brancolini et al., 2019; Panara et al., 2021; Montone & Mariucci., 2023; Maesano et al., 2023; Pezzo et al., 2023, Lavecchia et al., 2023). ~~The This~~ related active contraction, ~~affecting the Periadriatic region~~ is testified by historical seismicity (Boschi et al., 2000; Guidoboni et al., 2019; Rovida et al., 2022), ~~and by~~as well as ~~many numerous~~ observations derived ~~by from~~ geodetic (Bigi et al., 1992; D'agostino et al., 2008; Palano et al., 2020; Pezzo et al., 2020), geological, geophysical (Finetti & Del Ben., 2005; Fantoni &

Franciosi, 2010; Ghielmi et al., 2010; Tinterri & Lipparini, 2013; Casero and Bigi, 2013) and seismotectonic studies (Di Bucci and Mazzoli, 2002; Maesano et al., 2013; Brancolini et al., 2019; Panara et al., 2021; Montone & Mariucci, 2023; Carboni et al., 2024).

The subsurface offshore thrust faults and related folds in the study area ([Fig. 1](#)) are part of the latest contractional structures associated with the evolution of the Northern Apennines thrust belt. The contractional structures possess [a](#) similar geometry to that of the outcropping westward structures, where the chain is exposed (e.g. Mazzanti and Trevisan, 1978; Alvarez, 1999; Barchi, 2010). In the Northern Apennines in particular, previous [work-studies](#) suggested that at [least](#) two main sets of structures [coexist](#), namely the Umbria-Marche folds ("deep-seated - large - structures") and shallow imbricates ("shallow-seated - ~~small~~ ~~—structures~~~~small-structures~~") ~~coexist~~ (multiple décollements model - Massoli et al., 2006). These two sets of structures have different characteristics and significance. Weak décollements, located at different depths, influence the geometry and kinematics of the thrust systems. Such décollements largely govern the thrusts ~~s~~ [dimensions](#) and evolution, so that the deeper the décollement, the larger the wavelength of the structure (Barchi et al., 1998; Barchi et al., 2010). These considerations are supported by both field observations (e.g., Koopman, 1983; De Feyter, 1986) and former seismic interpretation works in the same region (Pieri and Groppi, 1981; Castellarin et al., 1985; Bally et al., 1986; Barchi et al., 1998; Pauselli et al., 2002) ~~and~~ [as well as in](#) further areas ~~in~~ [of](#) the Central Adriatic Sea. (e.g., Carboni et al., 2024).





80

Fig.1. Seismotectonic framework of the Northern Adriatic Sea. Red dots indicate recorded seismicity from 9th November 2022 (the Fano-Pesaro earthquake) until 1th of January 2025, including events with magnitudes higher-greater than Mw 1.7 (959 events). and the focal mechanism of the main shock (9th November 2022). The orange and yellow stars indicate the main shocks of the 9th November 2022 earthquake events, provided by INGV (INGV). Blue diamonds indicate the seismicity of the region derived from both instrumental and non-instrumental archived earthquakes from years 1269 to 2019, obtained from CPTI15-DBMI15v.4.0. (Rovida et al., 2022 and Locati et al., 2022). The focal mechanisms are from INGV (2022 eq and 2013 eq), Vannoli et al. 2015 (1930 eq). Seismogenic-The seismogenic sources are from DISS 3.3.0 (DISS Working Group, 2021), while-and the fault traces and Fault names (TTS, CTS, PTS and ETS) are from Maesano et al. (2023). The bathymetric contours are based on data from the EMODnet Bathymetry Consortium (2020). The seismic reflection profiles include public tracks from ViDEPI (light gray), representative lines S3 and S4 (green) from ViDEPI, as well as lines S1, S2, and S5 (blue) from ENI.

85

90

95 ~~Understanding The~~ the subsurface geological setting ~~of a~~ in a seismically active area is ~~hence crucial~~ essential not only for ~~the~~ ~~identification of~~ identifying the active causative fault segment, but also ~~to identify for~~ determining the lithologies involved in seismic faulting (e.g. Mirabella et al., 2008). In addition, the ~~position-spatial distribution~~ of these subsurface geological ~~bodies~~ units also affects the ~~distribution-configuration~~ of the ~~associated-different~~ seismic velocity ~~block~~ models, which are ~~fundamental~~ ~~critical in earthquake~~ for achieving more accurate earthquake location ~~studies-solutions~~ (Latorre et al., 2016).

This study focuses on ~~the~~ recent ~~Fano-Pesaro earthquake~~ seismic sequence ~~that~~ occurred in the southern portion of the Northern Adriatic (NA) Sea, about 25 km offshore from the coastal towns of Fano and Pesaro (Fig. 1). ~~The earthquake caused, which~~ ~~caused~~ damage along the entire coast of the Marche Region. This area ~~has~~ experienced significant seismic activity ~~starting~~ ~~from~~ since November 2022, culminating with a Mw 5.5 earthquake on ~~9~~ the 9th of November 2022. ~~One minute later, a Mw 5.2 earthquake followed the first event, approximately 8 km more to the south-southeast.~~ The focal mechanisms of ~~both~~ earthquakes ~~the main earthquake~~ indicate ~~ed~~ almost pure thrust-slip motion along a NW-SE striking fault. ~~No moment tensor solution has been computed for the Mw 5.2 event due to phase overlap and interference from the two events~~ (Pezzo et al., 2023). ~~By This earthquake sequence, at~~ the end of December 2024, ~~this earthquake sequence had~~ recorded over 560 aftershocks 105 larger than Mw 2 (<http://terremoti.ingv.it>).

In this study, an extensive investigation across an area of about 1400 km² of the Adriatic Sea offshore Pesaro and Ancona towns, has been carried out. A comprehensive data analysis has been accomplished across this region, in order to understand and shed light on the geological and structural settings, aiming to provide insights ~~on~~ into its tectono-stratigraphic evolution and ~~to its~~ seismotectonic character. Therefore, stratigraphic and geophysical analysis, as well as extensive seismic 110 interpretation, were carried out on selected wells and legacy reflection seismic profiles, including both unpublished (commercial) and freely available data stored in public databases (<https://www.videpi.com>). This study aims to demonstrate the importance of a thoughtful re-use and revision of such offshore data. This workflow is ~~mandatory-essential~~ to ~~shed light~~ ~~onto the subsurface geological settings of the area~~ ~~build up a reliable geological model to that can~~ be compared and integrated with seismicity, particularly because no surface outcrops are clearly available, and there ~~exist-are~~ well-known uncertainties 115 characterizing the offshore ~~earthquakes-earthquakes'~~ relocations. The joint use of seismic reflection profiles, calibrated with borehole stratigraphy, ~~provides the necessary framework to mitigate these limitations and improve the accuracy of the~~ ~~geological models~~ ~~interpretation~~.

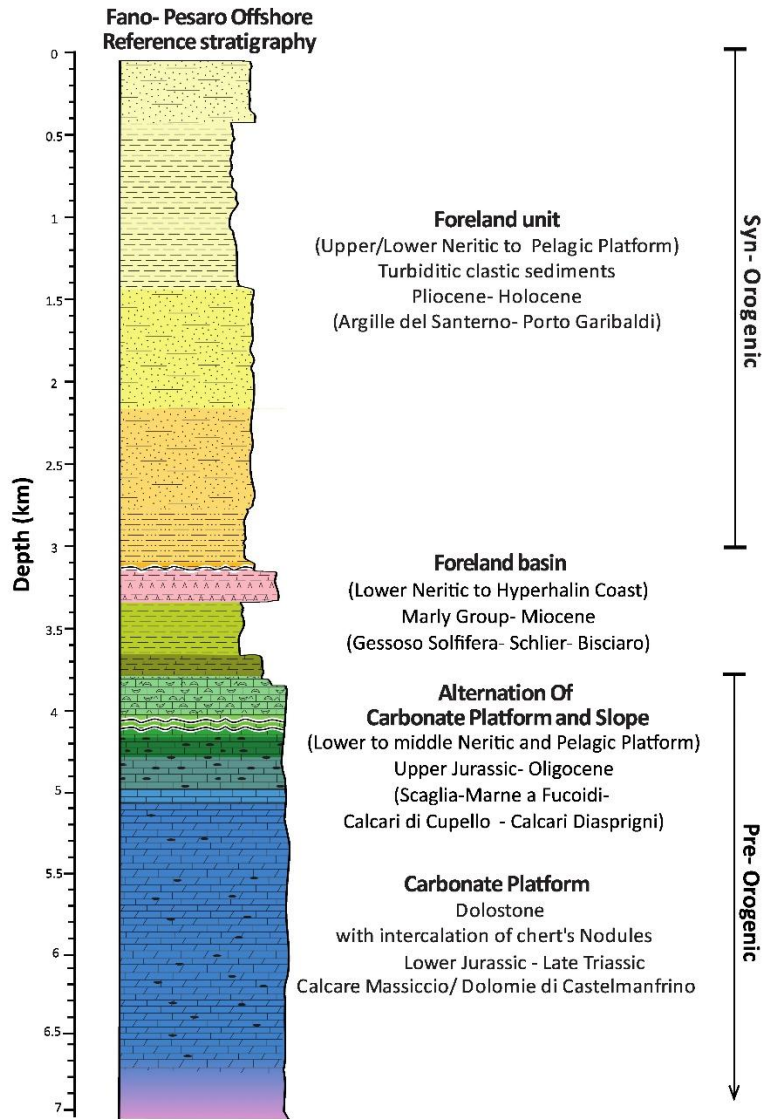
2. Geological, Structural settings and regional seismicity.

The NA Sea is predominantly composed of continental crust (Ollier & Pain., 2009; Piccardi et al., 2011) and represents the 120 deformed foreland of the surrounding orogenic belts, including the Apenninic belt to the West, the Dinarides-Albanides to the East, and the southern Alps to the North (Fig.1). The Adriatic Sea is composed of different stratigraphic units registering the initial drowning and the subsequent emersion of the Tethys margin (e.g., Finetti & Del Ben., 2005; Casero and Bigi, 2013). The initial rifting phase led to the deposition of ~~Permian-Anisian~~ Permian-Anisian sandstones interbedded with dolostones, limestones, gypsum and salt. During the Late Triassic, the normal faults accommodating the initial Tethys rifting, allowed the

125 deposition of evaporitic deposits and shallow-water carbonate sequences (Mattavelli et al., 1991; Geletti et al., 2008; Carminati et al., 2013; Wrigley et al., 2015). The further sea opening promoted the ~~growing-growth~~ of extensive carbonate platforms during the Lower Jurassic, which were subsequently buried by the deposition of Lower Jurassic–Palaeocene intraplateform pelagic carbonate succession (e.g., Centamore et al., 1992; Menichetti and Coccioni, 2013). The closure of Tethys marked the beginning of the compressional phase, which led to the formation of the Alps since the Cretaceous (e.g., 130 Dewey et al., 1989; Schmid et al., 2004; Stampfli & Borel, 2002; Handy et al., 2015), the Dinarides-Albanides since the Palaeocene-Eocene (e.g., Ustaszewski et al., 2010; van Unen et al., 2019; Schmid et al., 2020; van Hinsbergen et al., 2020), and the Northern Apennines since the Oligocene (e.g., Molli, 2008; Molli and Malavieille, 2011; Barchi, 2010; Caricchi et al., 2014; Carboni et al., 2020 a, b). The migration of both the Dinarides and Apennines towards the central axis of the Adriatic Sea (Channell et al., 1979), led to the deposition of upper Eocene–Quaternary sequences on their common foreland basin.

135 The stratigraphic succession includes a Mesozoic-Paleogene, pre-orogenic, passive margin succession, deposited on the southern side of Western Tethys, and a Neogene-Quaternary, syn-orogenic succession, deposited on the flexured foreland of the Northern Apennine. A reference stratigraphic column is shown in Figure 2, illustrating the main units derived from Pesaro Mare ~~04~~ and ~~W+WI~~ boreholes drilled in the study area (Fig.1).

The uppermost unit includes up to ~ 3200 meters of Pliocene–Quaternary foreland turbiditic clastic sediments, ranging from 140 Upper/Lower Neritic to Pelagic Platform environments, and includes the Argille del Santerno (AS) and Porto Garibaldi (PG) formations. These sediments transgressively ~~overly-overlie~~ a relatively thin Miocene Marly Group succession, deposited in the distal part of the foreland. This succession includes formations of the ~~Messinian's-Messinian~~ Gessoso Solfifera (GS) (relatively thin), Schlier (SCH) and Bisciaro (BIS) formations. The pre-orogenic multilayer, spanning from the Late Triassic to the Early Miocene, lies beneath the overlying successions. This interval consists of Meso-Cenozoic carbonate deposits alternating 145 between platform and slope facies, indicative of deposition in Lower to Middle Neritic and Pelagic Platform settings. Key formations include the Upper Jurassic to Oligocene Scaglia (SCA), Marne a Fucoidi (FUC), Calcari di Cupello (CDC), and Calcari ~~dDia~~-Asprigni (CDU), as well as Lower Jurassic dolostones, such as the Calcare Massiccio (MAS) and Dolomie di Castelmanfrino (DCM). Compared to the Umbria-Marche Basin, this succession shows significant differences, notably the interlayering of platform facies with pelagic deposits in the Late Jurassic to Early Tertiary interval. The Triassic succession of 150 the Anidriti di Burano Formation (BF) consists of alternating dolostones, anhydrites, halite, and gypsum, and ~~aet-acts~~ as regional décollement horizons (Casero and Bigi, 2013). Beneath this succession, the pre-Mesozoic crystalline basement of the Adriatic microplate forms the foundational framework (Vannoli et al., 2014). Due to the limited availability of deep wells, direct data on the thickness and depth of these deeper units remain sparse, necessitating reliance on seismic interpretation.



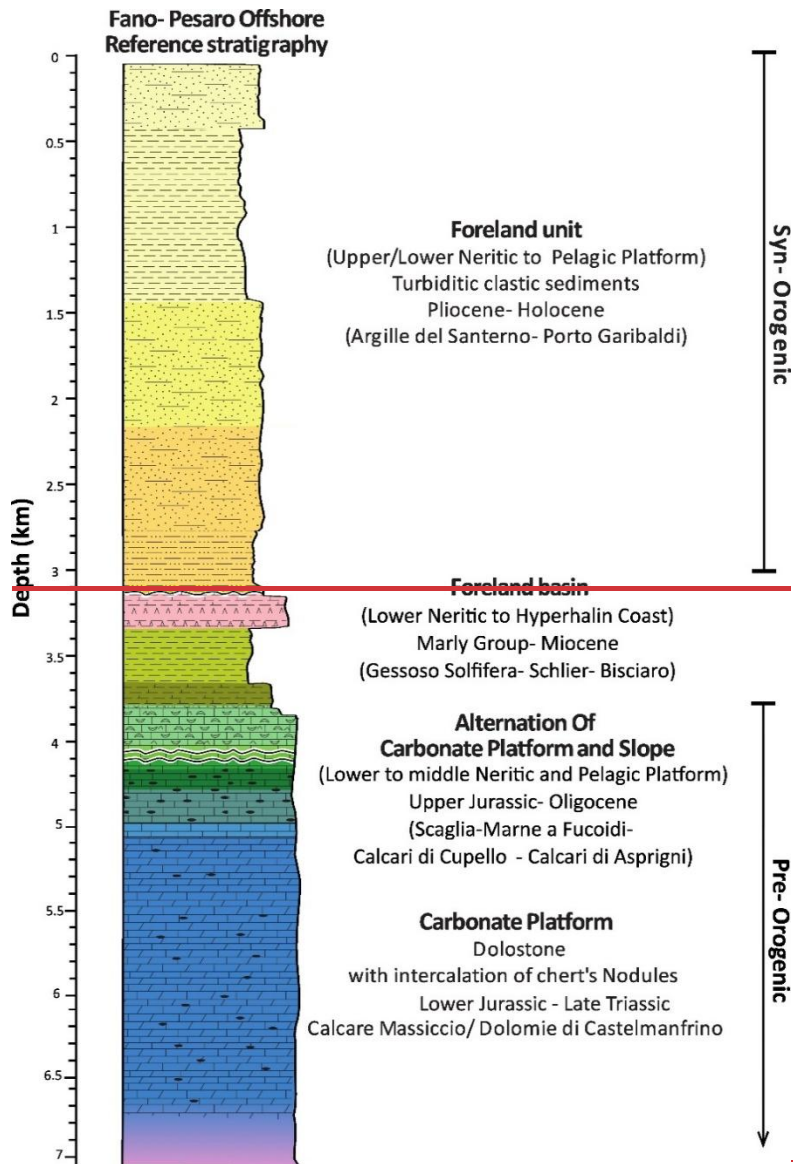


Fig. 2. Reference stratigraphic column for the Pesaro-Fano offshore area (from the Late Jurassic to Holocene sedimentary succession), derived from two representative boreholes (~~W1 and~~ Pesaro Mare 04 ~~and W1~~, location in Fig. 1).

160 The NA is characterized by a high sedimentation rate, that evolved throughout the Pliocene and Pleistocene, reflecting changes in the depositional environment and regional subsidence. During the Pliocene (5.33–2.58 Ma), sedimentation rates were estimated at 1–2 mm/year in both the Po Plain area and the NA Sea (Ghielmi et al., 2010, 2013; Amadori et al., 2020; Maesano et al., 2023). In the Po Plain area, these rates increased to over 2.5 mm/year during the Calabrian stage (1.8–0.78 Ma) with measured values ranging from 2.83 ± 0.19 mm/year to 2.14 ± 0.21 mm/year (Maesano & D'Ambrogi, 2016). However,

165 ~~sedimentation rates progressively decreased throughout the Middle (0.78–0.126 Ma) and Upper Pleistocene (0.126–0.0117~~
~~Ma), reaching a minimum of 0.39 ± 0.05 mm/year in the last 0.45 Myr. This decrease reflects the transition to continental~~
~~deposition and a general reduction of accommodation space in the basin, while also recording the effect of ongoing regional~~
~~subsidence during the Pleistocene (Maesano & D'Ambrogi, 2016). that in the Po Plain area reached more than 2.5 mm/year~~
170 ~~during the Calabrian, decreasing down to ~ 0.4 mm/year in the Upper Pleistocene (Maesano & D'Ambrogi, 2016). In the NA~~
~~Sea, it is estimated in 1–2 mm/year in the Pliocene (Amadori et al., 2020; Ghielmi et al., 2013, Maesano et al., 2023).~~ The high
sedimentation rate, ~~and~~ the absence of a clear seafloor deformation found on bathymetric and seismic reflection data (Di Bucci
& Mazzoli, 2002), along with the generally low-to-moderate magnitude of instrumental seismicity ($M_w < 4.0$, before 2012),
have ~~ve~~ fueled the scientific debate on the recent activity of the external Northern Apennines. Contrary to slightly more internal
sectors (e.g. Conero area, Cuffaro et al., 2010), most authors agree that the tectonic deformation in this external area might be
175 hidden by such a fast sedimentation rate. In the NA Sea, the shortening rate is estimated ~~in~~ ~~at~~ 1–2 mm/year until the Calabrian
times, although some studies suggest spatial variations and a progressive temporal decrease (Maesano et al., 2015; Gunderson
et al., 2018; Amadori et al., 2020; Panara et al., 2021). Within the same area, some authors, using GNSS data from offshore
hydrocarbon seabed-anchored platforms, recently calculated a present-day shortening rate, to be about 1.5 mm/year (Palano et
al., 2020; Pezzo et al., 2020, 2023). The offshore tectonic deformation characterizing the study area has been imaged ~~by~~
180 ~~using~~ seismic reflection profiles, showing that the tectonic structures are organized in multiple blind thrusts with associated
anticlines (Argnani, 1998; Bigi et al., 1992; Fantoni & Franciosi, 2010; Ghielmi et al., 2010; Maesano et al., 2023). Such
reverse faults are buried below thick Plio-Pleistocene marine and continental deposits and likely rooted at depth along a
common basal décollement (Bally, 1986; Panara et al., 2021; De Nardis et al., 2022).

The debate about the recent activity of the external Northern Apennine associated to such blind thrusts has been revived during
185 the last ~ 15 years, as a few important earthquake sequences have been recorded before the 2022 sequence (Maesano et al.,
2023; Lavecchia et al., 2023): one in the 2012 and a second in the 2013, onshore in the Pianura Padana (northern Italy) and
offshore southern of Ancona in Marche region, respectively (Mazzoli et al., 2015; Maesano et al., 2013; Burrato et al., 2012;
Scognamiglio et al., 2012; Tertulliani et al., 2012; Pezzo et al., 2013; Tizzani et al., 2013; Bonini et al., 2014; Nespoli et al.,
2018). Additionally, a revision of the historical seismicity extracted from the available seismic catalogues, reports sequences
190 encompassing mainshock events of $M_w \geq 5.5$, whose epicentres location is mapped either offshore or onshore the coastline
(e.g., 30 October 1930, M_w 5.8 at Senigallia (Vannoli et al, 2015), Fig. 1). These earthquakes have been mainly caused by
active thrust faults and produced several induced effects, as well as victims and extensive damages within the Marche Region
(Guidoboni et al., 2019; Rovida et al., 2022; and Locati et al., 2022). All these recent seismic events ~~have~~ stimulated recent
studies integrating different disciplines, providing new information, evidence and constraints to the active tectonic setting of
195 the outer Northern Apennines.

3. Fano-Pesaro earthquake: State of the Art

The Fano-Pesaro earthquake sequence began on November 9, 2022, with a Mw 5.5 mainshock. One minute later, a Mw 5.2 earthquake occurred approximately 8 km to the south-southeast of the mainshock. Before this, only one smaller event (ML 2.8) was recorded roughly two months before the mainshock, and no foreshocks immediately preceded the sequence. This abrupt activation caused notable damage along the central Adriatic coastline, drawing significant attention to the area's complex tectonic structures.

Most authors identify that the Adriatic domain ~~is being~~ mainly governed by compressive tectonics, with thrust-related deformation playing a dominant role (e.g., Pauselli et al., 2006; Maesano et al., 2013; 2023; Sani et al., 2016; Lavecchia et al., 2023), although others suggest the region is primarily affected by active strike-slip tectonics, with minor thrusts that are occasionally reactivated (e.g., Di Bucci and Mazzoli, 2002; Mazzoli et al., 2015).

Since the Fano-Pesaro 2022 earthquake sequence, ~~new research~~ several studies ~~has~~ have been conducted to better map the ~~existing regional~~ structures and ~~recognize the~~ identify the possible seismogenic ~~faults through~~ faults. These studies have employed several various hypotheses and scientific approaches as well as ~~improving the accuracy of~~ seismicity relocation, to achieve this goal (Maesano et al., 2023; Pezzo et al., 2023; Lavecchia et al., 2023; Pandolfi et al., 2024; An et al., 2024).

Maesano et al. (2023) ~~were among the first that performed~~ perform a review and reinterpretation of public seismic reflection profiles (CROP and ViDEPI profiles), alongside comparisons with earthquake locations and aftershock distributions from INGV. These authors suggested that the Fano-Pesaro Offshore earthquake sequence took place ~~on along~~ a relatively small section (25–40 km²) of the buried Cornelia Thrust System (CTS), a buried thrust structure situated at the edge of the Northern Apennines ~~(Fig. S1)~~. The affected segment covers an area of approximately 25–40 km² within the larger CTS fault, which itself extends roughly 28 km in length and 10–15 km in width. The CTS is estimated to have a total fault surface area of about 300 km², making it capable of generating earthquakes up to magnitude 6.5. They also proposed a control by pre-existing normal faults and associated structural highs of the subducting Adria monocline (Amadori et al., 2019; Livani et al., 2018). Their work confirms the CTS being an active fault, It is roughly 300 km² in size, which could produce ruptures up to magnitude 6.5 and may trigger nearby faults.

Shortly Pezzo ~~after~~ Pezzo et al. (2023) characterized the seismic sequence in space and time, using data from the INGV monitoring system, GNSS-constrained coseismic slip, and public seismic reflection profiles (ViDEPI). ~~They observed~~ Their interpretation ~~shallow~~ identified shallow buried anticlines in the upper 5–6 km of the crust with ramps dipping 20°–35° extending from a deeper, regional basal décollement with a westward dip of 1°–7°. Based on the distribution of relocated aftershock events, the authors interpreted a 15 km long striking seismogenic fault patch, dipping 24° SSW and seismically active at depths of 5–10 km. Using the HypoDD relocation method, they refined the mainshock's position, revealing it to be 4.4 km farther south and at a deeper depth of 8 km than previously reported in the INGV catalogue. Their mainshock relocation generated a 4.4 km shift to the south and a depth increase down to 8 km.

Lavecchia et al. (2023) expanded this picture by investigating the broader lithospheric scale deformation (De Nardis et al. 2022), examined-analyzing the multi-scale geometries of slowly deforming continental regions (SDCR) in eastern Central Italy, focusing on lithospheric scale deformation (De Nardis et al. 2022). They suggested the presence of a shallow megathrust (T1, ~ 20 km to a few km deep) which represents the basal detachment of the external fold-and-thrust domain of the Adriatic Arc. These authors propose the T1 splay, named Bice thrust, extending ~ 30 km with a listric geometry (dip angle ~ 40°– 20°, seismogenic depths ~ 7– 11 km) and converging at depth with the Cornelia Thrust. Upon associating the first mainshock (Mw 5.5) with the central and southern part of the Bice thrust, they interpret the second event (Mw 5.2) as due to the subordinate activation of the northern part of the Cornelia Thrust. Following this study, Pandolfi et al (2024) conducted a probabilistic seismic hazard analysis for the Adriatic Thrust Zone (ATZ).

More recently, An et al. (2024) proposed a new workflow to relocate the Fano-Pesaro seismicity, revealing sharper earthquake clusters in a depth range of between 2–12 km depth, with Their analysis estimated a best-fit fault dip of about approximately 30° towards the south-southwest. In comparison to the results available in the INGV catalogue, they presented a sharper earthquakes-earthquake cluster closer to the shoreline, mapping a geometry coherent with the available focal mechanisms as well as with the horizons interpreted-interpreted in seismic reflection profiles.

Finally, Costanzo et al. (2024) presented a new catalogue of the 2022-2023 Adriatic Offshore Seismic Sequence obtained through machine learning-based processing. His relocation placed the ML 5.5 mainshock approximately 0.5 km above the Cornelia fault. compared to the INGV catalogue, this event was shifted 0.44 km southward and 1.2 km deeper. Similarly, the ML 5.2 event was relocated approximately 0.6 km deeper and slightly northwest of its position in the INGV catalogue.

The different interpretations show that the seismogenic structure is not clearly understood at the moment. While Maesano et al. (2023) and Lavecchia et al. (2023) propose new models that differ in identifying the causative faults, other studies (Pezzo et al., 2023; An et al., 2024 and Costanzo, 2024) focused on seismotectonic analysis and the relocation of seismicity, correlating the events with existing models. While-Despite differences in the approaches, results and interpretations on thrust geometries, dimensions, depths and structural relationships, -might differ, all-all of the above-mentioned studies agree that the 2022 earthquakes are related to an average $\sim 30^\circ$ dip, southwest-dipping thrust fault, located in the frontal part of the Northern Apennines. However, different opinions remain about which thrust could be the causative structure for the recently recorded seismicity.

255 4. Data and methods

The findings outlined in this paper are based on the interpretation of four deep wells (Table 1) and a set of seismic reflection profiles, comprising 8 crosslines and 3 tielines, -covering an area of approximately 1400 km², five of which are described and discussed in detail. Initially, No-no digital data (e.g. SEG-Y files) were available to be used for enhancing the quality of the dataset (e.g., Barchi et al., 2021, Ereoli et al., 2023, Carboni et al., 2024), but . Instead, all the seismic reflection profiles were provided as digital images, scanned from hard paper copy, in pdf-PDF format. Three of the selected seismic reflection profiles

and a key-borehole, kindly provided by the Italian Energy company Eni S.p.A. under a confidential agreement, are unpublished. The other boreholes and seismic reflection profiles were retrieved from publicly available datasets from ViDEPI databases (<https://www.videpi.com>; <https://www.crop.cnr.it>) (Figs. 1 and 2, Table 1), along with industrial exploration reports and maps, which have been deeply reviewed. In this study, these scanned images were digitized using the MATLAB code developed by Sopher (2018) to generate SEG-Y files, which were then slightly reprocessed and enhanced to improve their quality and interpretability of the seismic data (e.g., Barchi et al., 2021; Ercoli et al., 2023; Carboni et al., 2024).

A workflow, including different steps to gather and analyse all the data and ancillary information, has been set up:

1. *Data preparation*: data organization, quality control (QC), digitalization, georeferencing and importing into a geoscience multi-discipline integration software. 2D and 3D visualization of seismic reflection profiles, wells stratigraphy (formation tops), log images, and seismicity. This workflow incorporates several specialized software tools: e.g. QGIS for managing geospatial data, a MATLAB code (based on the methodology of Sopher, 2018) for digitizing seismic profiles, Petrel and Move platforms for seismic interpretation and velocity modelling, and OpendTect software for conventional data processing. Further details on the processing workflow are illustrated in Figures S1 and S2 of the supplementary materials.
2. *Data integration*: stratigraphic correlation among the wells' tops and logs to identify a local seismic stratigraphy, well-to-seismic well-to-seismic tie analysis and seismo-stratigraphic interpretation.
3. *Velocity model building*: a key well sonic log (Table 1, [Fig.3c](#)) was used to extract velocities for Pleistocene and Pliocene formations, whilst literature velocities ([Bally et al., 1986; Maesano et al., 2013, 2023; Montone & Mariucci, 2023](#)) were adopted for deeper layers (older than Late Miocene).
4. *Time to depth conversion*: horizons, faults and surfaces were converted to depth, and the correlations were extended and verified across a broader area.

Table 1. List of datasets (Sp= Spontaneous Potential, Res= Resistivity, Sn = Sonic). The star* marks the unpublished data, obtained under a confidential agreement, the hashtag# reports the public data downloaded from the Italian database ViDEPI.

Seismic profiles				Wells		
Type	Name	Length (Km)	Notes	Name	Depth	Logs
Cross line (NE-SW)	S1*	18	Intersected by W1 well	W1*	4300 m	Sp, Res
	S2*	11.5	Adjacent to the main shock (134 m)		Reached the Lower Cretaceous (Calcarei Di Cupello (CDC) Fm).	
	S3# (B-402)	30	/	Tamara 01#	3191 m	Sn, Sp, Res
	S4# (SV-167-13)	21	Intersected by Cornelia well	Pesaro Mare 04#	4258 m	

Tie line (NW- SE)	S5*	22	Adjacent to Pesaro mare -Mare 04 well		Reached the Lower Jurassic Dolostone (MAS Fm).	
				Cornelia 01#	3976 m Reached the Lower Jurassic Dolostone with Chert (Non defined ~ MAS Fm).	Sp, Res

285

5. Results

5.1. Wells' stratigraphy

The wells' stratigraphy was digitized, ~~and~~ analysed to identify common geological characteristics (e.g., stratigraphy, lithology, discontinuities, petrophysical properties derived from the logs) and trends (formation thickness, spatial continuity) among the wells. After reviewing and correlating the lithological and structural information among all the data, a reinterpretation of the wells' stratigraphy has been accomplished and displayed in Figure 3. In the latter, the analysed wells are displayed sequentially, moving from the northwest to the southeast of the study area (Table 1, red arrow in Fig.3a). The data ~~has been~~ summarized, aiming to clearly show the tectono-stratigraphic correlation among the four wells, highlighting the spatial variation and gaps due to the presence of erosional and tectonic discontinuities (Fig.3b). ~~Aiming to~~ To support a deeper understanding of subsurface geology within the study area, such well information was spatially extrapolated along the available seismic reflection profiles, by correlating them with the interpreted TWT (Two-Way Travel Time) seismic horizons ("well- to-seismic tie", Bianco, 2014) and fault sets. ~~From a lithostratigraphic standpoint, five major tectono-stratigraphic units were identified across four wells (Fig. 3):~~

AS unit (Holocene–Upper Pleistocene): A siliciclastic marine turbidite system composed of fine sandstones, shaly sandstones, and interbedding of shale and silty shale.

PG unit (Lower Pleistocene–Pliocene): This unit is separated from AS by a top-lap unconformity, dated Top Gelasian (Fig. 4), referring to early Pleistocene, older than 1.8 Ma. The Gelasian turbidites within the upper part of PG consist of silty shales with interbedded shales at the top, transitioning to fine sandstones and shaly sandstones in the lower part.

Messinian Marly group (GS-SCH-BIS; Upper Miocene): Comprising shales and marls interbedded with siltstones, carbonates, and minor gypsum deposits associated with the Messinian salinity crisis. The top of this unit is defined by a major unconformity marking the top Messinian surface interpreted as a subaerial exposure surface linked to tectonic uplift or sea-level drop.

SCA group (Oligocene–Upper Cretaceous): Made up of marly limestones interbedded with clays and cherts, attributed to the Scaglia succession. The unit thickens southeastward, consistent with deposition in a flexurally subsiding foredeep setting.

Carbonate platform units (FUC–MAS–DCM; Cretaceous–Jurassic): These include thick intervals of massive limestones and dolostones with variable chert and marl content.

310

Well-by-well stratigraphic characterization reveals distinct stratigraphic and structural features across the study area:

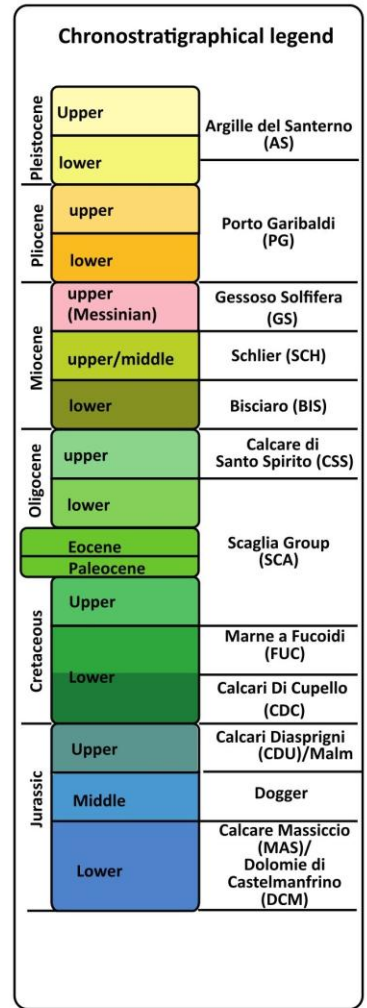
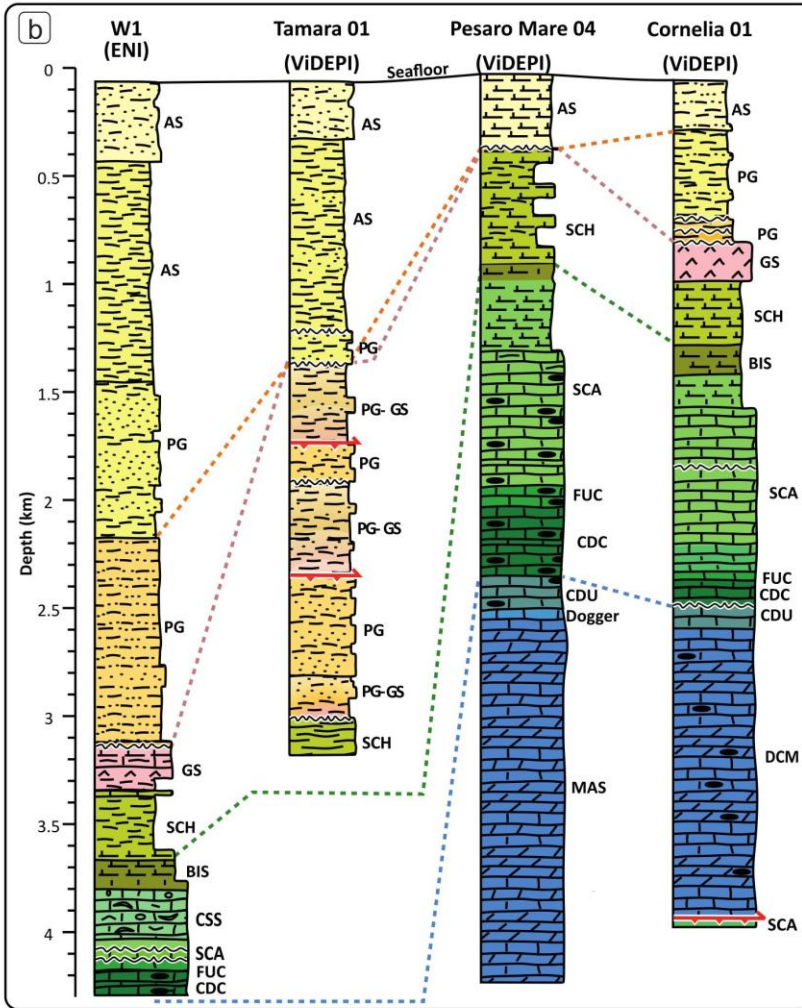
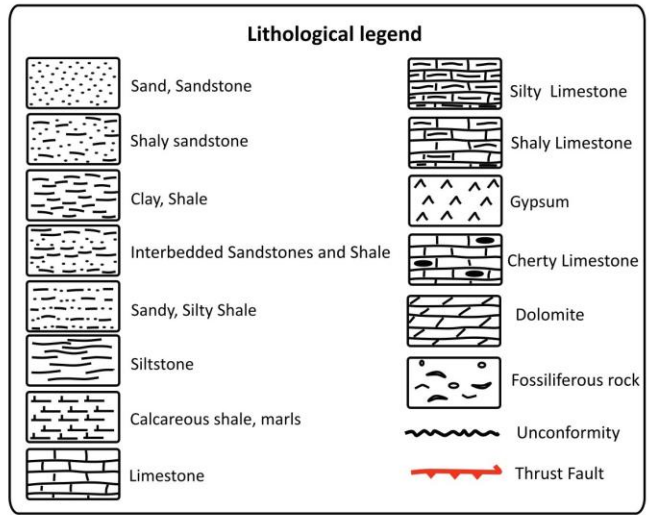
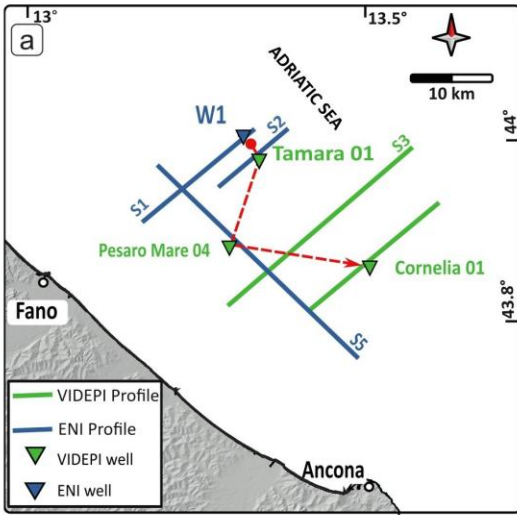
The W1 well intersects the easternmost segment of the seismic profile S1, ~~containing and contains~~ 160 m of Lower Cretaceous carbonates. Within this well, three erosional ~~boundaries-unconformities are-have been~~ identified, corresponding to the top Messinian ~~(between the PG and GS units) at a depth of 3151 m,~~ ~~middle-lower~~ the lower Oligocene (within the SCA unit) at a depth of 4070 m ~~Paleocene,~~ and the Lower Cretaceous tops ~~(between the SCA and FUC units) at a depth of 4154 m~~ (Fig.3).

The Tamara 01 well ~~is~~ located approximately 600 m southeast of ~~the~~ seismic profile S2 and near the ~~epieenter-epicentre~~ of the MW 5.5 Mw mainshock of the 9th November 2022. ~~It,~~ provides valuable sonic log data for deriving interval velocities and conducting well-to-seismic tie analysis. Projected orthogonally onto the eastern segment of the S1 and S2 seismic profiles, ~~the~~ Tamara 01 well penetrates the upper Miocene SCH Formation for about 176 m. The well exhibits four erosional unconformities and two tectonic boundaries. Erosional unconformities have been identified at several stratigraphic levels ~~The erosional boundaries are identified:~~ within Lower Pleistocene ~~(between the As and PG units) at a depth of 1217 m,~~ top of the Upper Pliocene (within the PG unit), ~~-At 1912 meters, marking both the top of the Upper Pliocene PG unit and the base of the Lower Pliocene of another PG and at two levels marking the tops of the Upper Pliocene (1370 and 1912 m) unit. And the last erosional unconformity occurs top of the Upper Messinian (between GS and SCH units) one level marking the top of the Upper~~ Miocene, located at a depth of 3015 m. The two tectonic boundaries are recognized from the repetition of the Miocene-Pliocene sequences at depths of 1743 and 2345 m, respectively (Fig.3).

The well Pesaro Mare 04, situated approximately 1 km southwest of the S3 profile, was projected ~~orthogonal-orthogonally~~ onto it. The well penetrates the sequence down to the Lower Jurassic, encompassing 1729 m of dolomitized MAS. Notably, an erosional ~~boundary-unconformity~~ corresponding to the top of the Miocene top (between SCH and AS units) is documented in the well stratigraphy at a depth of 372 m (Fig.3).

The Cornelia 01 well, located in the southeastern part of our study area, intersects the seismic profile S5. It penetrates Jurassic dolomitized carbonates, which are originally referred to as an *undefined* formation based on the lithological variability and uncertainties in variations and on the reported depositional environment; ~~however~~ However, considering their stratigraphic position beneath the Marne a Fucoidi and Scaglia Calcareo formations, and their overall characteristics as shallow-water platform carbonates, this unit is interpreted in this study as equivalent to the Dolomie di Castelmanfrino (DCM) Formation. This correlation is consistent with similar successions identified in other Apennine sectors, such as the Montagna dei Fiori area, where comparable dolomitized Jurassic sequences have been described and attributed to the DCM (Ronchi et al., 2003; Murgia et al., 2004; Bencini and Martinuzzi, 2012), it is equivalent to the Dolomie di Castelmanfrino (DCM) formation. This ~~The~~ Cornelia 01 well exhibits five erosional ~~boundaries-unconformities~~ corresponding to the tops of the Upper Pliocene (within PG unit) at a depth of 686 m), Lower Pliocene (within PG unit) at a depth of 738 m), Upper Miocene (between GS and PG units) at a depth of 790 m), Upper Cretaceous (Within SCA unit) at a depth of 1833 m), and Lower Cretaceous (between CDU and FUC units) at a depth of 2478 m). Additionally, a tectonic boundary is reported approximately 30 m from the bottom of the well. It is interpreted as a thrust splay, whose offset results in the repetition of the Early-Lower Cretaceous succession.

345 (Fig.3)-The well was drilled only into the upper part of this repeated interval (Lower Cretaceous succession), and no data are available for the deeper successions (Fig.3).



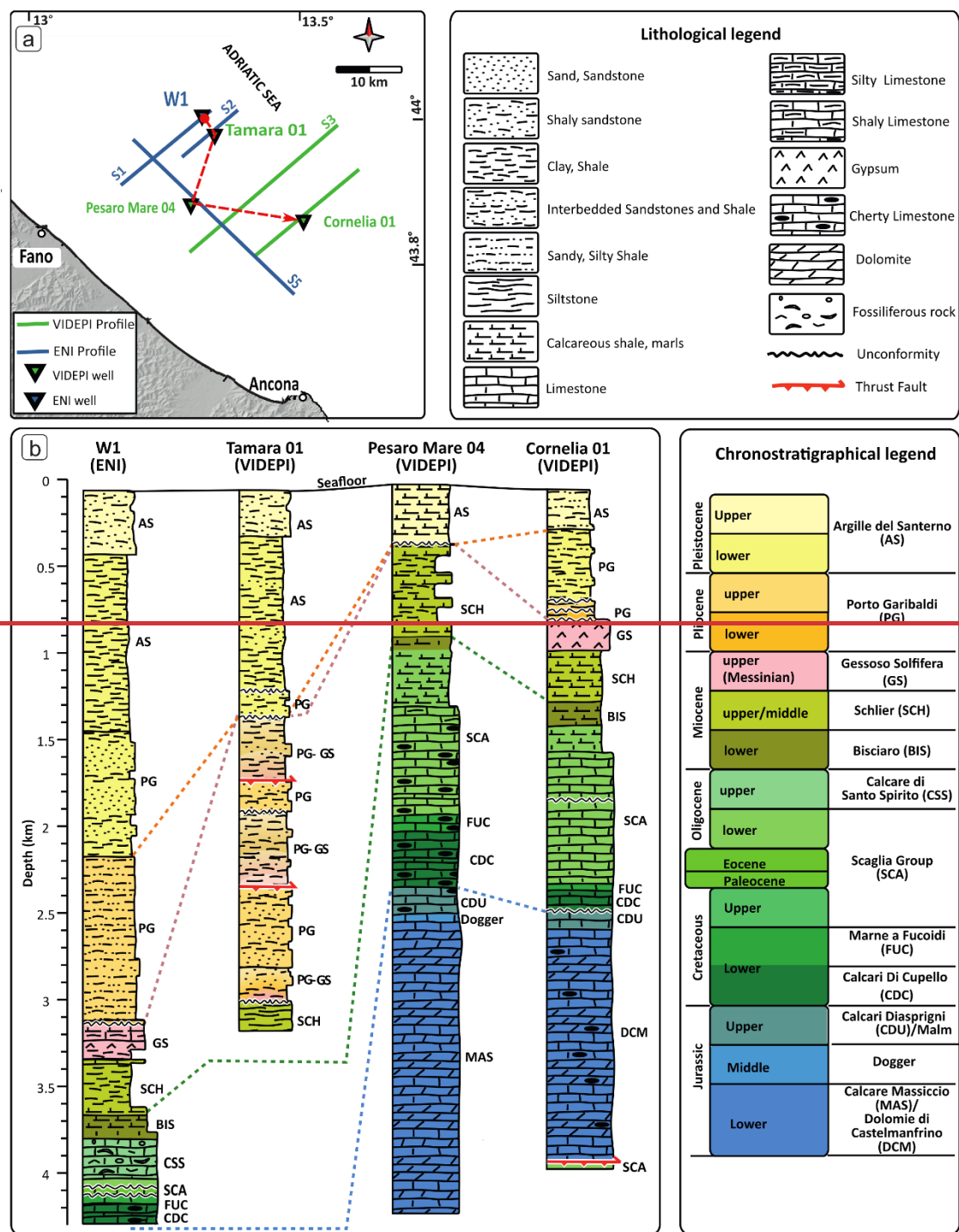


Fig. 3. a) Location map showing the position of the analysed wells. b) Schematic stratigraphic columns of the wells, reinterpreted from the original data in the ViDEPI database and arranged spatially from northwest to southeast (red arrow in Fig. a).

From the global analysis of the four wells' data across the study area (Fig.3), the Pliocene-Quaternary successions (AS and PG units) show a significant thinning from ~ 3100 m thickness in the northwest to 400– 700 m in the southeast, as recorded in Pesaro Mare 04 and Cornelia wells, respectively. Within southeastern wells (Pesaro Mare 04 and Cornelia 01), ~~this succession,~~ the Pliocene-Pleistocene sedimentary sequence is frequently incomplete. Notably, in the Pesaro Mare 04 ~~well,~~ situated on a structural high, the Pliocene succession (PG unit) is entirely absent, with a direct transition from Miocene deposits to Quaternary sediments. Conversely, in the basin areas, such as the W1 well, a more complete sequence spanning the lower to upper Pliocene is preserved. This sequence is characterized by alternating sandy and clayey layers, often interbedded with marly components. This sequence unconformably overlies the Messinian (GS) evaporites, which are identified exclusively in the northwestern (W1) and southeastern (Cornelia 01) wells of the study area. These evaporites are associated with a Messinian paleo-high that persisted as a subaerially exposed feature for the majority of the Pliocene (Report 1508, ViDEPI).

The lithological analysis of the Meso-Cenozoic carbonate successions within the studied wells reveals a carbonate platform that underwent progressive deepening, testified by the combination of detrital and dolomitic limestones, interspersed with frequent cherty nodules and marly intercalations, particularly in the lower sections. The Triassic succession (BF), which typically consists of evaporites and dolostones in the central Apennines (e.g., Umbria-Marche and Sabina Pelagic Basins), is not intercepted by the studied wells due to their limited depth. However, its presence is inferred from nearby Alessandra 01 well (See location in Fig.1), located slightly to the east, which represents the deepest borehole drilled in this region, and is in this study area is almost entirely composed of dolostone facies reported by (Bally, (1986), and Carminati et al., (2013) and Scisciani & Esestime (2017), as reported by the analysed wells. This is also shown by the Alessandra 1 well, located slightly to the east, which represents the deepest borehole drilled in this region (Bally, 1986; Carminati et al., 2013). As the succession transitions into the Middle Jurassic and extends to the Paleogene, the limestones gradually give way to marly layers, ~~again characterized by typical nodular structures.~~ Additionally, clastic intercalations are observed, suggesting sedimentary inputs from the erosion of adjacent structural highs. Notably, the thickness of the SCA Group increases significantly from the northwestern to the southeastern studied wells (Fig.3).

5.2. Seismic stratigraphy and time -to depth conversion.

By correlating and calibrating the stratigraphy of Tamara 01 and W1 wells with all the available seismic profiles, we have identified five primary seismic units (SUs), bounded by four prominent, easily traceable key-reflections. These units exhibit distinct geophysical signatures, such as variation in the reflection amplitude, period and geometry. The analyzed seismic profiles follow SEG normal polarity, meaning that an increase in acoustic impedance is represented by a peak, while a decrease corresponds to a trough. The SUs are discussed in the following from top to bottom (Fig.4 and details within the Supplementary Table S1).

~~The SU1 corresponds to the Holocene-Upper Pleistocene turbiditic deposits (AS unit).es (The uppermost part of SU1) comprise fine sandstones, shaly sandstones, and interbedding of shale and silty shale pertaining to AS. SU1 consists of four~~

385 distinct seismic sub-units (SU1 a, b, c, d), each one characterized by a different seismic signature (see supplementary Table S1). SU1 ~~is a, b are~~ characterised by ~~seismic facies from~~ continuous to ~~semi-discontinuous~~ semi-discontinuous, horizontal and parallel reflections, with low to high amplitudes; ~~the While the bottom lower part~~ SU1 c, d ~~display displays~~ continuous to semi-continuous, ~~Eastward~~-dipping reflections, with medium to high amplitudes (Fig.4 and Supplementary Table S1). The total thickness of ~~this unit~~ SU1 gradually increases north-eastwards, ~~ranging~~ from ~ 0.2 s to ~~0.3-1.5~~ s TWT across the study area (Fig.4 and Supplementary Table S1). ~~This~~ ~~Thickening pattern is consistently observed in all interpreted seismic profiles (Figs. 5 and 6).~~

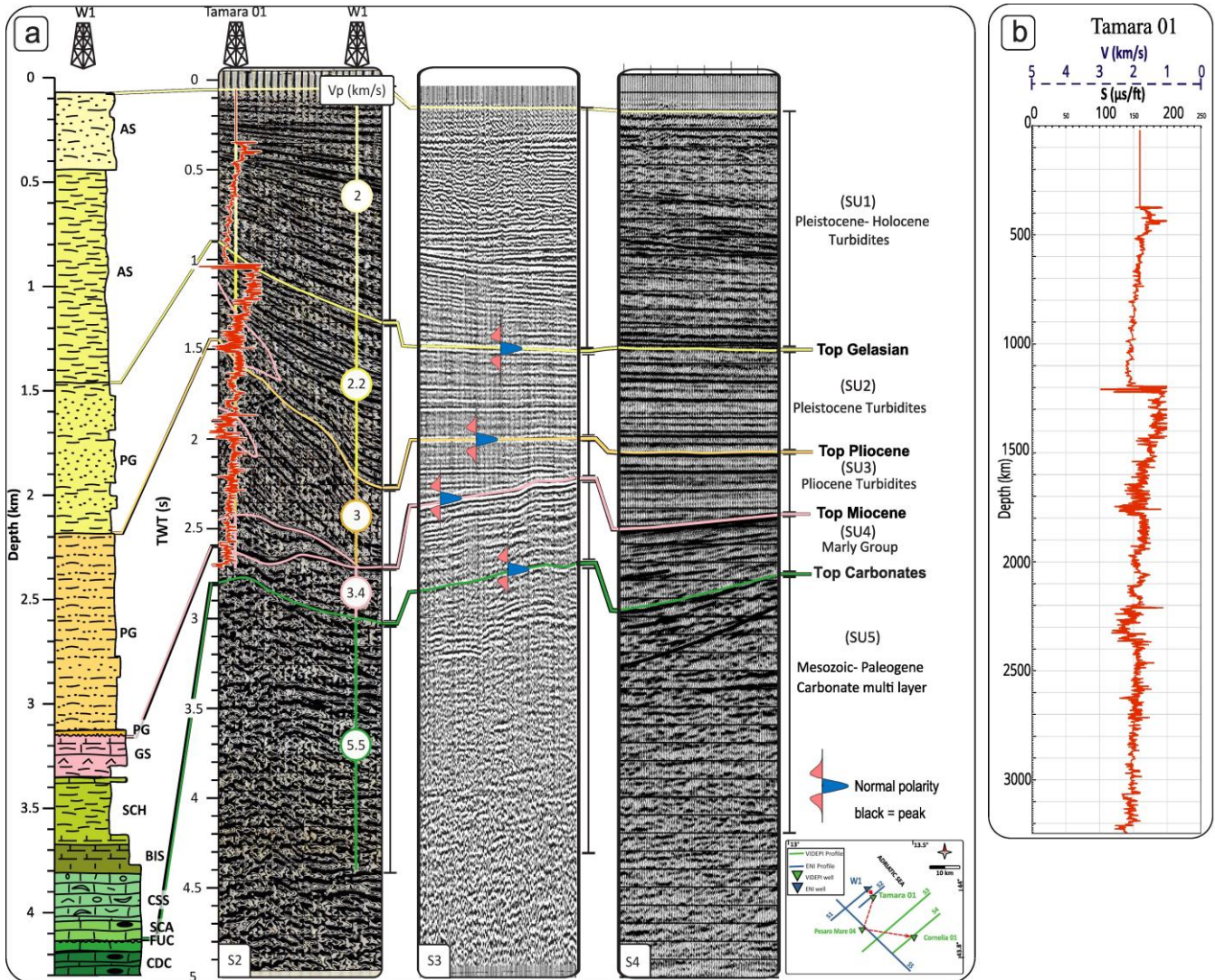
390 SU2 ~~corresponds to the lower Pleistocene turbiditic deposits (PG unit) and~~ is separated from SU1 by a top-lap unconformity, dated to Top Gelasian (~~older than 1.8 Ma;~~ (Fig. 4) ~~referring to early Pleistocene older than 1.8 Ma. The Gelasian turbidites within the upper part of PG consist of silty shales with interbedded shales at the top, transitioning to fine sandstones and shaly sandstones in the lower part.~~ The thickness of this unit gradually increases from ~ 0.2 s in the SW to 0.6 s in the NE. ~~Similar to SU1, this Thickening pattern is consistently observed in all interpreted seismic profiles (Figs 4, 5 and 6). Within SU2, we identified two sub-units (SU2 a, b), each one characterized by distinct seismic signature.~~ The uppermost sub-unit (SU2 a) ~~part of this unit shows displays~~ continuous, NE-dipping parallel reflections, with medium to high amplitudes. In contrast, the lower sub-unit SU2 b ~~part~~ features semi-continuous, parallel, and sub-horizontal reflections (Supplementary Table S1).

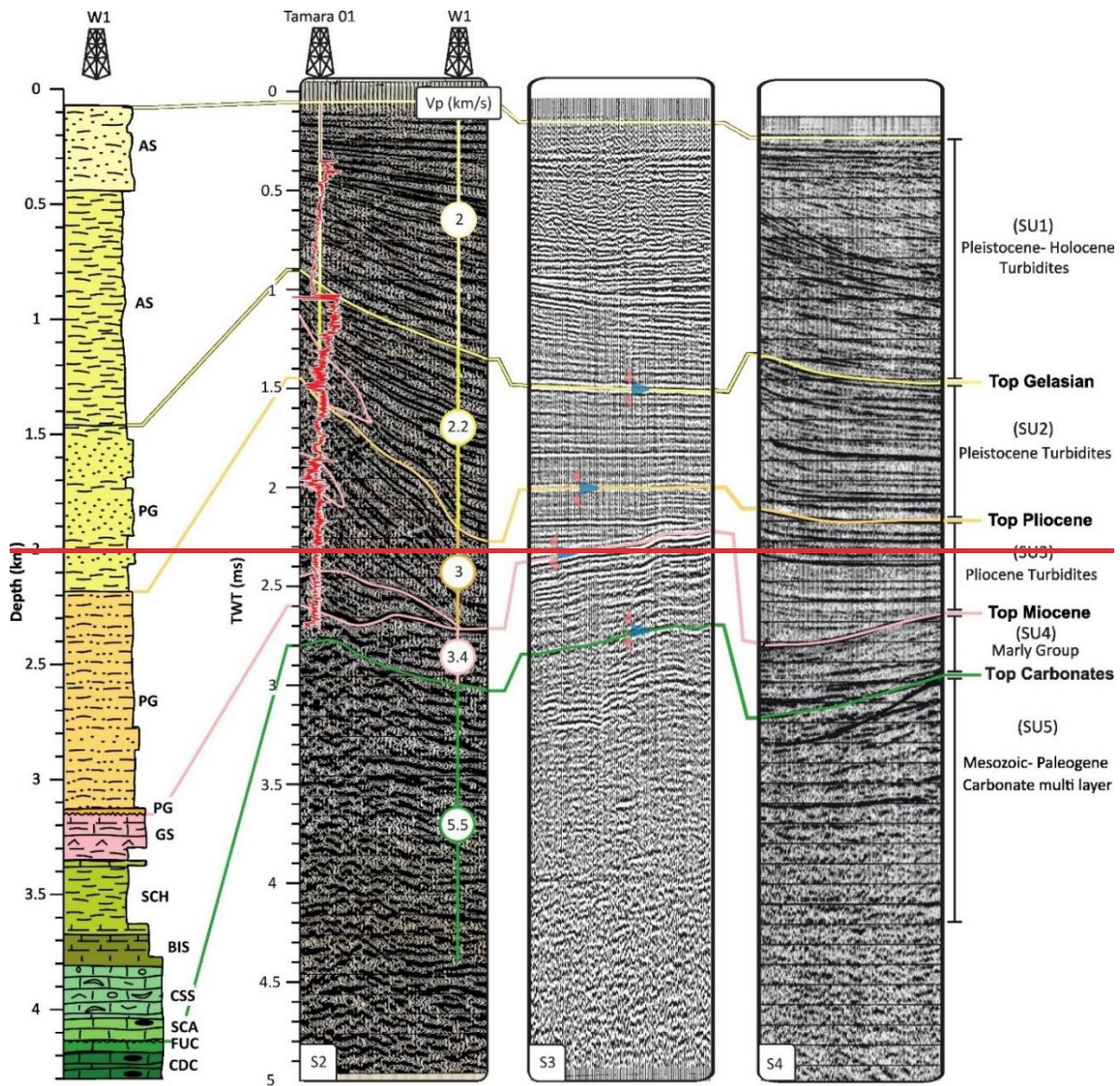
400 The SU3 ~~represents the~~ Pliocene ~~turbidite~~ turbidite (~~deposits unit~~ SU3) ~~within and is located in~~ the lower part of PG ~~are composed of silty marls intercalated with medium to very fine grained sandstones.~~ The subunits (unit SU3 a, b, c) ~~unit displays~~ distinct reflection patterns. The uppermost ~~part subunit (SU3 a) of it~~ exhibits continuous, horizontal, parallel reflections with high amplitude, while the ~~other subunits (SU3 b and SU3 c) middle and lower parts of it~~ show discontinuous to semi-continuous, sub-parallel reflections with low to medium amplitudes. The ~~thickness of this unit varies~~ thickness ~~of this unit varies~~ across different sections, ~~is~~ ranging from a few ms to 0.4 s (Figs. 4, 5, and 6).

405 The SU4 ~~represents the~~ complex Miocene succession (SU4) ~~and is observed found~~ within the GS, SCH, and ~~BISBIS Fms., are composed of shales and marls interbedded with siltstones, carbonates, and minor gypsum deposits.~~ This marly group displays continuous, parallel reflections with high amplitude and high dominant frequency in the narrow uppermost part ~~and creates distinct and sharp reflections in the seismic sections. The~~ rest of the unit presents continuous to discontinuous, sub-parallel reflections with medium to high amplitude (Supplementary Figs S1, S2 and Table S1). ~~–This seismic unit progressively deepens from southwest to northeast (Figs 4, 5 and 6). The high amplitude and dominant frequency within this unit create distinct and sharp reflections in the seismic sections.~~

415 The SU5 unit ~~represents the~~ Mesozoic-Paleogene carbonate multilayer (SU5) ~~unit and~~ corresponds to the SCA, MAS and DCM Fms. and represents the deepest ~~recognized~~ units identified in the study area (Figs 4, 5 and 6). ~~The unit consists of limestone and dolomitized limestone, with intercalations of marls and chert nodules.~~ Notably, it exhibits a substantial thickness of over 1 s. The reflections within this unit display a discontinuous, sub-parallel pattern with low to medium amplitude and are marked by some continuous, high amplitude and well-recognizable reflections which are related to the top of the SCA and FUC fms. (Mirabella et al., 2008; Porreca et al., 2018; Barchi et al., 2021).

For the depth conversion, a velocity model has been built, by integrating new interval velocity values derived from the sonic log of the Tamara 01 well (down to the Late Miocene turbidites) with literature velocity data (e.g., Bally et al., 1986; Maesano et al., 2013, 2023; Montone and Mariucci, 2023). Bi-dimensional velocity models were initially built up along each single profile, with a focus on the shallower area (down to the Top SeagliaSCA). This workflow was then extended across a tri-dimensional workspace, encompassing later variations driven by all the picked-interpreted horizons and faults-fault surfaces, and considering some control points correlating with corresponding to the well data from located a broader area. Such a velocity model was later refined in its deeper portion (down to the Jurassic carbonate units) and used to carry out the final conversion from the time to the depth for all the selected seismic profiles. Further details on the velocity models are provided in the Supplementary Table S2.





430

Fig. 4. a) Seismic stratigraphy of the study area (colored lines) calibrated using the Tamara 01 and W1 wells; (see Fig. 1 for well locations and Fig. 3 for stratigraphy column abbreviations). Vp indicates the average P-wave seismic velocity. The displayed values represent averages of the original velocities reported in the last column of Supplementary Table S2, which were derived from sonic log interval averages for the younger succession up to and including the SCH unit, and from published sources for the deeper intervals. Additional details are provided in the text and supplementary Table 2. b) Digitized sonic log from the Tamara 01 well, showing raw slowness (Δt , $\mu\text{s}/\text{ft}$) / row velocity (Km/s).

435

5.3. Seismic interpretation

440 To provide an accurate representation of the subsurface geological and structural features within the research region, five seismic profiles have been selected to ~~carried-carry~~ out the seismic interpretation. Their location and details are ~~reported-shown~~ in Figures 5, 6 and Table 1, while the uninterpreted versions can be found in the supplementary material (Figs. S1 and S2). The dataset includes four SW-NE-oriented “*cross-lines*” (S1, S2, S3, and S4) and one NW-SE oriented “*tie-line*” (S5). The SW-NE profiles cross the two major anticlines present in the area, namely the northern Pesaro Anticline (PA) and the southern
445 Cornelia Anticline (CA), developed at the hanging walls of SW-dipping thrusts, named Pesaro thrust (PT) and Cornelia thrust (CT) (Figs 5 and 6).

The whole interpretation of seismic profiles has been realized by using a ~~pseudo--~~tri-dimensional correlation of key reflect~~orsions~~ions picked along the single seismic profiles, by tying reflectors picked on intersecting lines with respect to seismic-stratigraphic units obtained from the well-tie analysis. In this section, the description of the seismic profiles is done from
450 northwest to southeast. The profiles are described considering the increasing TWT (s) and their ~~along-line~~along-line distance (km).

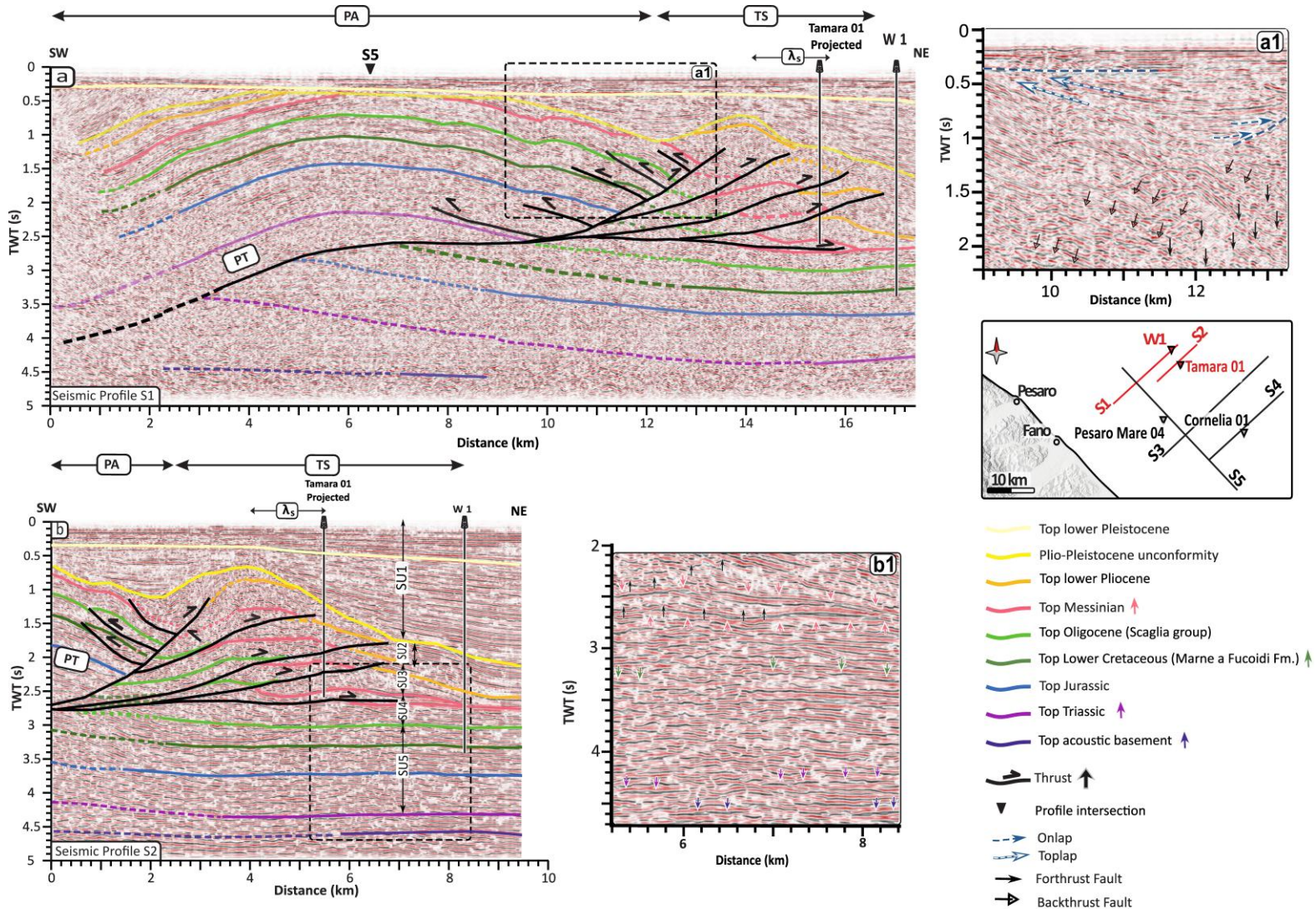
The seismic profile S1 ~~in Figure 5a~~ is dominated by the east-verging PA, characterized by a long wavelength of ~~~ 13-12~~ km (0–12 km distance, Fig. 5a). The PA geometry is traceable from ~ 0.2 s down to ~ 2.5 s, and it is particularly evident following the interpreted Top Jurassic to Top Messinian ~~reflections-reflectors~~ (blue and pink colours, respectively). To notice that the
455 Top Messinian ~~reflection-reflector~~ is not traceable ~~in-at~~ the culmination of the PA anticline, due to erosion; in addition, a set of minor folds characterizes the PA forelimb (9–12 km distance range). The more internal minor folds, closer to the crest zone of PA, affect a thicker succession, ranging from the Jurassic to the Pliocene, and are traceable through key reflectors such as the Top Jurassic (blue colour), Top Lower Cretaceous (dark green colour), Top Oligocene (light green colour), and Top Messinian (pink colour). In contrast, the more external folds deform shallower successions, mainly involving
460 the Messinian units and the overlying Pliocene sediments (Fig. 5a, 5b). Further to the northeast, between 12 and ~ 17 km distance, a complex antiformal structure (wavelength ~ 5 km) folds the Plio-Pleistocene unconformity reflect~~orion~~ion (dark yellow colour; ~~Fig.5a~~). This antiformal stack involves a set of minor imbricates, with wavelength < 1 km, detached above the Top Carbonates (Oligocene) ~~reflection-reflector~~ (light green colour; Fig. 5a, b). The antiformal stack is here referred to as the Tamara structure (TS), drilled by the Tamara 01 well. The PA and TS are separated by a short wavelength (~ 4 km) syncline
465 (~ 9–13 km distance), which is infilled by sub-horizontal ~~reflections-reflectors~~ interpreted as lower Pleistocene sediments, onlapping and toplapping onto the Plio-Pleistocene unconformity (Fig. 5a, inset a1). In the northeastern part of the profile (~13–17 km), a clear increase in the apparent dip angle and thickness of the Pleistocene succession ~~reflections-reflectors~~ is visible (Fig. 5a, 5b). Both the PA and the TS are interpreted to be situated in the hanging wall of the SW-dipping main PT thrust. The hinge zone of PA is located on top of the main PT ramp, located within the Mesozoic succession; this ramp links
470 its deepest part with the shallowest, flat portion at ~2.5 s (Fig. 5a). However, in this forelimb sector, a set of imbricate forethrusts and backthrusts have been interpreted departing from PT (Fig. 5a, inset a1, 5b). These backthrusts have been

associated with the minor folds described above on the PA forelimb (~9–13–12 km distance range). Such backthrusts are ~~detached-imbricated along from the shallower, most internal PT ramp innermost secondary ramp of the PT, whereas the forethrusts. On the other hand, the set of imbricate forethrusts, build-builds up the shorter wavelength TS, and they are all~~ detached along the PT shallower flat are all imbricated from and detached along the shallower flat of the PT. The three imbricates displace up to the Top Messinian and the Top ~~lower-Lower~~ Pliocene ~~reflections-reflectors~~ of at least ~0.1 s TWT, but not the Plio-Pleistocene unconformity, which is only folded. The presence of such imbricates is also interpreted and constrained by the Tamara 01 well stratigraphy, clearly showing two repetitions of the Top Messinian. Further constraints on the PT geometry are derived from a set of parallel sub-horizontal ~~reflections-reflectors~~ observed between 2.5 s and 3.5 s (5–18 475 17 km range); they are discordant with the shallower reflectorions, especially in correspondence with the main ramp, between 3 and 8–9 km distance, where they look slightly E dipping. These reflectorions would represent the PT footwall succession, up to the Top Messinian (Fig. 5a).

The seismic profile S2 (Fig. 5b) ~~covers only a small portion of the PA forelimb, including the shallowest flat of the PT, and gives-provides~~ a clearer picture of the TS imbricates; ~~the PT footwall reflectors, previously described in S1, are also visible here and appear more continuous and better traceable (Fig. 5b, inset b1).~~ Projecting the Tamara 01 well and picking the Top Messinian reflectiorions, the presence of three imbricates within the TS, which produce three repetitions of the Messinian and Pliocene successions, have been interpreted. The imbricates are detached on the shallow PT flat (~2.5 s TWT), which produces a further repetition of the Top Messinian reflectiorion (pink colour). In the south-western part of S2, again, the minor folds driven by the backthrusts mapped in S1 are observable ~~in the north-easternmost part of the PA forelimb~~. Within S2, like in S1, the 485 growth deposition of the Pliocene succession is also observed in the northeastern part (apparent E-dip), and the syncline separating the PA and the TS, again characterized by parallel sub-horizontal reflectiorions associated with the Pleistocene unit (Fig. 5b).

495

500



505 **Fig. 5.** Interpretation of S1 and S2 seismic profiles. a) S1, the northernmost section in the study area, crosses the left hinge zone of the PA and reveals variations in its structural style. This profile intersects with seismic section S5 at a ~ 6.1 km. The geometry of the PA is evident by using the Top Messinian, Top Oligocene and Top Lower Cretaceous reflectors. The section also shows the shallow-seated TS developed laterally to the South-Eastern termination of the PA. b) S2 shows the enhanced comprehension of the TS's underlying structure. Four imbricated thrust zones of the PA forelimb and the repetition of Messinian- middle- lower Pliocene successions are observable (uninterpreted images provided in supplementary materials, Fig.S1). Insets a1 and b1 show detailed interpretations. λ_s = wavelength of the small structure; PT= Pesaro Thrust; PA= Pesaro Anticline; CA= Cornelia Anticline; TS= Tamara Structure; SU= Seismic Stratigraphic Unit.

510

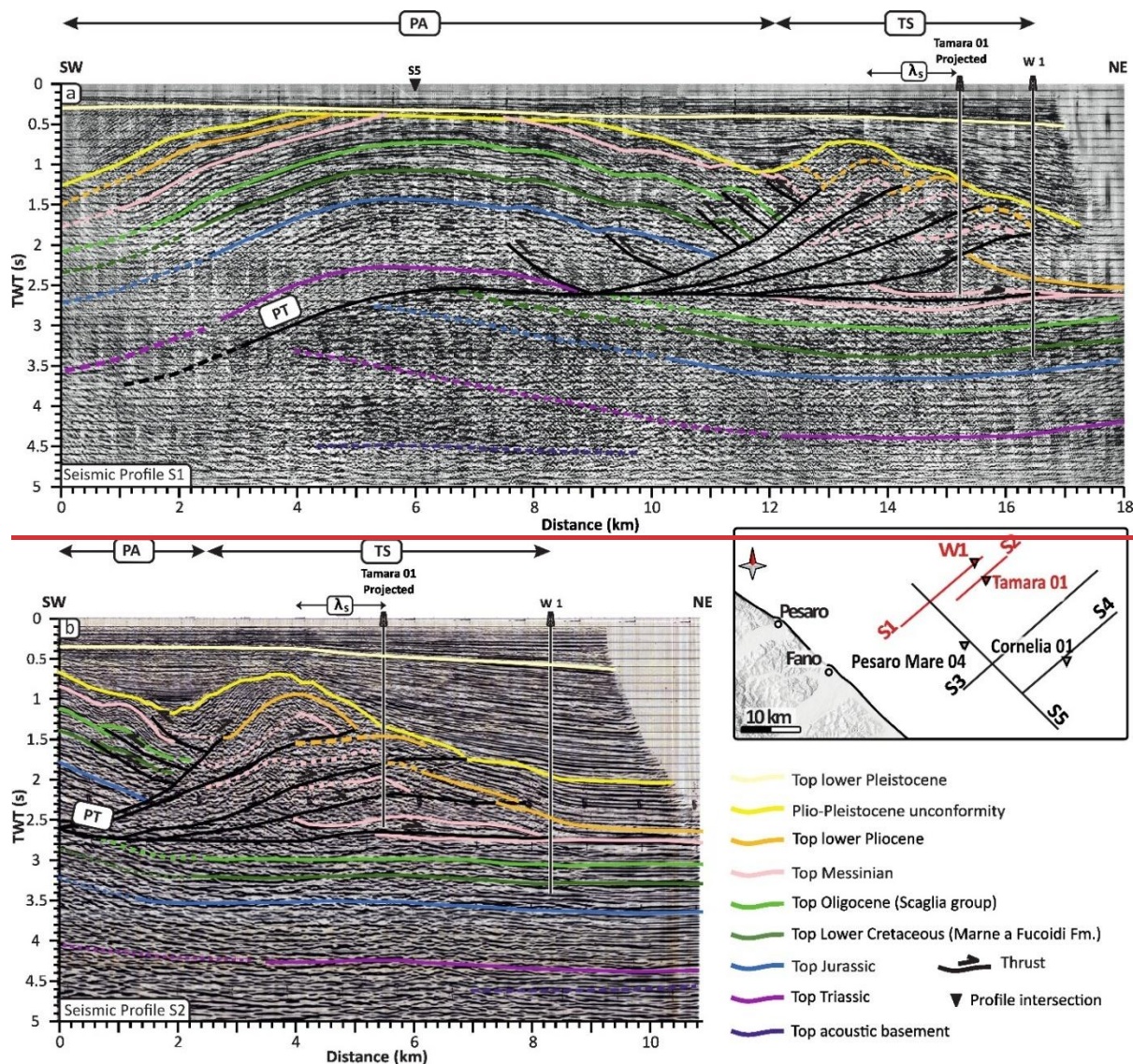


Fig. 5. Interpretation of S1 and S2 seismic profiles. a) S1, the northernmost section in the study area, crosses the left hinge zone of the PA and reveals variations in its structural style. The geometry of the PA is evident by using the Top Messinian, Top Oligocene and Top-Lower Cretaceous reflections. The section also shows TS shallow seated structure developed laterally to the South-Eastern termination of the PA. b) S2 shows the enhanced comprehension of the TS's underlying structure. Four imbricated thrust zones of the PA forelimb and the repetition of Messinian–middle–lower Pliocene successions are observable (uninterpreted images provided in supplementary materials; Fig.S1).

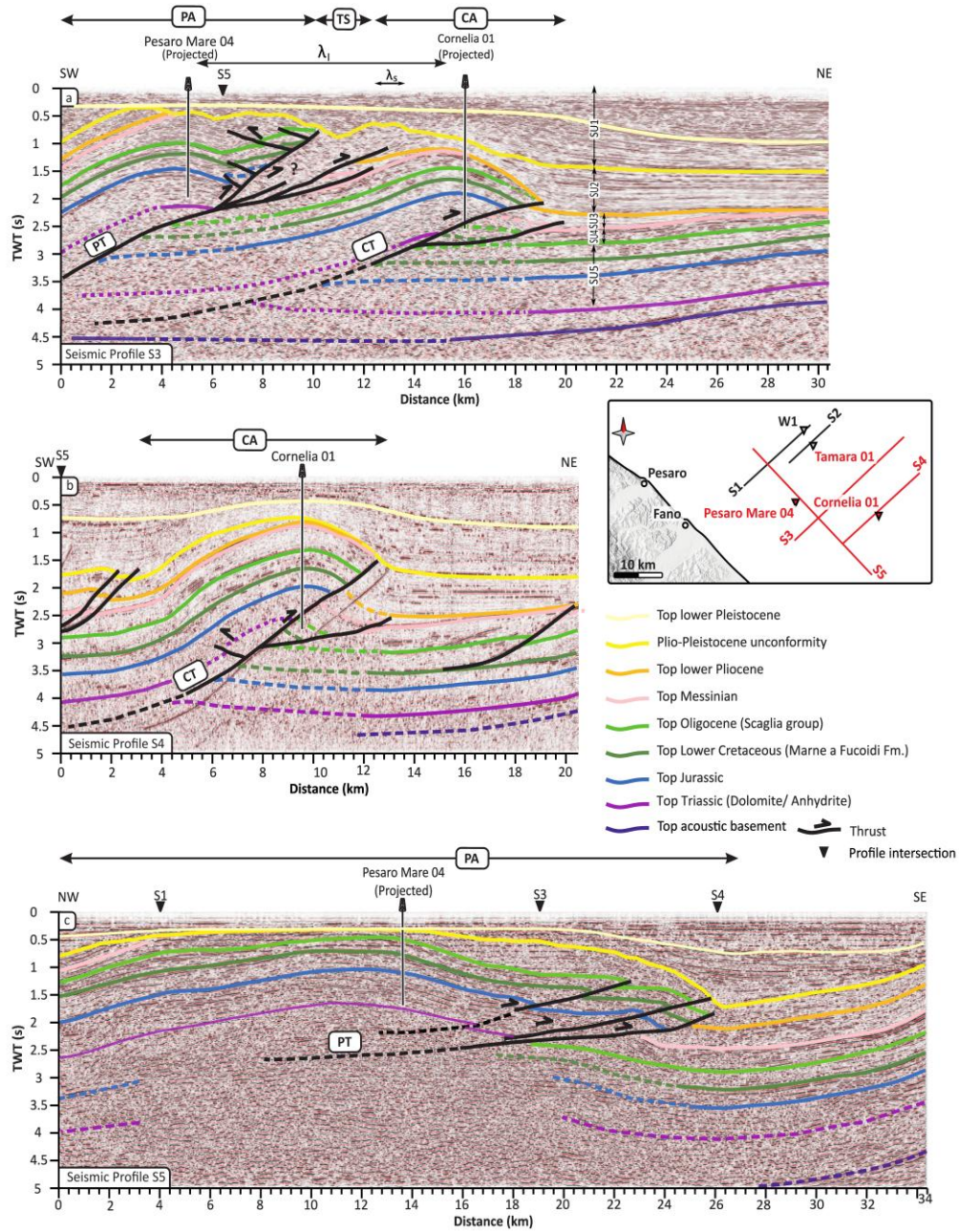
515

520

The seismic profile S3 (Fig. 6a) provides an excellent view of the structural relationships between the two main structures of the area: the main thrusts PT and CT with their related anticlines PA and CA. The PA is displayed in the southwestern part of the profile (0–10 km distance range). Its geometry can be easily appreciated by following the Top Jurassic to the Top Messinian reflectorions (blue and pink colours, respectively); the latter is again partially eroded in the axial zone. A few smaller antiformal

structures located at the PA forelimb, as already observed in S1 and S2 (Fig. 5), are again interpreted as being driven by small backthrusts. This profile also shows a strongly reduced size of TS and a steepening of the PT, here partially overlies the western flank of another anticline, identified as CA. More north eastwards, the latter appears as an asymmetric NE-verging anticline, traceable from ~ 0.8 s down to ~ 3 s. This anticline is interpreted as being related to the underlying CT, whose location is constrained by the Cornelia 01 well. The CT displaces the Meso-Cenozoic succession up to the Top lower Pliocene reflector (orange colour), while the Plio-Pleistocene unconformity (yellow colour) appears only folded. The CT footwall is recognized following the Top Jurassic to the Top Messinian reflectors, which are interpreted as slightly parallel and W-dipping until around 18 km distance at ca. 3 s. The CT is interpreted to comprise also a small synthetic thrust, developed at its footwall, which produces a further repetition of the Top Scaglia SCA Group and Top Messinian reflectors. More to the northeast, we observe a shallower and thicker package of growth strata, interpreted to comprise Pliocene to Quaternary deposits, traceable from approximately 0.5 s to ~2 s TWT between ~16 and ~23 km distance (Fig. 6a).

The seismic profile S4 (Fig. 6b), located at the southernmost extent of the study area, offers valuable insights into the internal structure of the CA and intersects the Cornelia 01 well, providing key stratigraphic correlations. In contrast to S3, the PA is not present in this seismic section. The CA is represented by an asymmetric NE-verging anticline (as already also observed in S3), extending from ~0.5 s to ~3.5 s, and is prominently displayed between 3 km and 14-13 km distance. This anticline is defined by the folded reflectors from the Top Jurassic-Triassic up to the Pliocene-Pleistocene unconformity reflections (blue purple and to yellow colours), situated within the hanging wall of the underlying CT. The latter, like in S3, offsets the Meso-Cenozoic succession up to the Top lower Pliocene reflector (orange colour); however, in this section, located at the crest zone of the CA (Fig. 1), the structure exhibits the maximum height compared to S3, which lies in the northwestern hinge zone, resulting in a larger displacement of the Top Lower Pliocene reflectors (from 1.25 to 2.0 s in S4 versus 2.1–2.2 s in S3; Fig. 6a, b). A small synthetic thrust is again observed in the footwall of the CT, which results in the repetition of the Top Oligocene (Top SCA Scaglia Group) and Top Messinian reflectors over 9 to 14 km, extending to ~2.7 s. In the northeastern part of this section, the interpreted Pliocene to Quaternary deposits (SU1 and SU2), close to the end of the forelimb of the CA (~13 km distance), are thicker than at the similar location in S3, with the top of the Pliocene reflector located at ~2.5 s in S4 versus ~2.1 s in S3. Additionally, S4 reveals minor fore-verging thrusts in both the southwestern and northeastern sectors of the section (Fig. 6b, at distance ranges 0–3 km and 15–20 km, respectively). While the two west-dipping convergent thrusts observable to the south-west of the CA intersect and slightly displace the Messinian until the Plio-Pleistocene unconformity, the minor thrust to the northeast of CA is detached at the top of the Lower Cretaceous (~ 3.5 s to 2.2 s), displacing the overlying sedimentary successions including deposits from the Upper Cretaceous (dark green) to the Messinian and the Lower Pliocene deposits (orange colour, Fig. 6b).



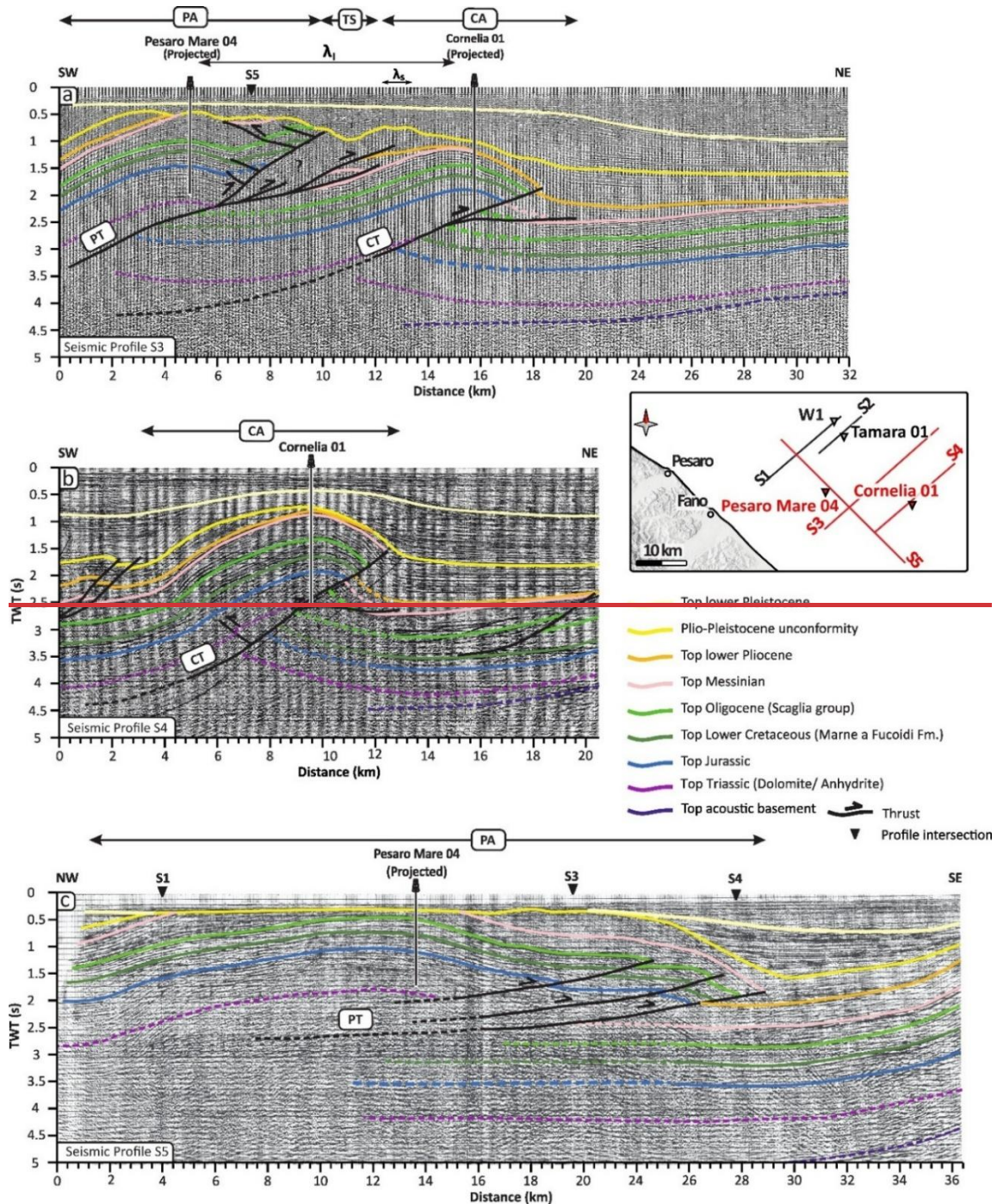


Fig. 6. Interpretation of seismic profiles S3, S4 and S5. a) Section S3 crosses the transition zone of PA and CA structures. The geometries of the anticlines are identified by using the key reflectors (See the legend). However, in this section, the main reflectors in the TS are not clearly traceable (the area marked with a question mark). b) Section S4 is the southernmost section that shows the CA. The doubling of the Mesozoic-Paleogene carbonate multilayer is observable in the frontal part of the CA. c) Section S5 is a tie line, crossing the crest zone of

560 the PA (Uninterpreted images provided in supplementary materials, Fig.S2). λ = wavelength of the large structure; other abbreviations are as in Fig. 5

The seismic profile S5 (Fig. 6c) serves as a tie line, crossing the crest zone of the PA and situated approximately 500 m from the Pesaro Mare 04 well. This profile provides extensive areal coverage (~36 km), and intersects the S1, S3, and S4 seismic profiles. It is essential for understanding the structure of the PA and for conducting a ~~3D~~-correlation of interpreted horizons among the aforementioned cross-lines. The geometry of the PA is identifiable from ~0.5 seconds to ~2 seconds, being particularly prominent following the reflectors Top Jurassic (blue) and the Top Messinian (pink). The Top Messinian reflector is visible in the northwestern and southeastern hinge zones of the PA, but is clearly absent in the axial zone (~4–~~15–20~~ km distance) due to erosion. The central portion of the PA (~12–29 km distance range) exhibits a stack of imbricate thrust slices between ~1.5 s and ~2.5 s. These slices are characterized by semi parallel, closely spaced reflectors (Fig. 6c). The PA lies in the hanging wall of the PT, and it is significantly uplifted, forming a semi-symmetrical structure. In contrast, the footwall remains relatively undeformed. These three interpreted thrust faults cut across both the Mesozoic and Cenozoic successions. In the northwestern hinge zone of the PA, no clear displacement has been observed and interpreted within the primary reflectors. Moving to the southeast, starting from ~ 16 km along the profile, growth deposition of the Pliocene-Pleistocene succession (SU1 and SU2) becomes increasingly evident (Fig. 6c). The profile highlights the superimposition of the Meso-Cenozoic sedimentary sequence over the Messinian reflection picked on top of the footwall, with clear evidence of duplication.

The described interpretations carried out on the seismic profiles in TWT, have been then converted to depth, by using the integrated velocity model illustrated in figure 4.

580 6. Discussion

The integration of both a new set of unpublished and publicly available seismic profiles with borehole data allowed us to highlight the presence of deep-seated and shallow-seated tectonic structures, involving different lithologies and detached ~~in~~ correspondence of along different décollements. This structural setting defines the geometry, dimension and segmentation of the main compressional structures, and ultimately their seismotectonic significance. Depth-converted profiles are used to discuss the possible link between the deep-seated tectonic structures and the seismicity of the area, with a focus on the 2022 seismic sequence (Fig.7). Three depth-converted seismic profiles, S1, S3 and S4 have been selected, being the most representative, on the base of on the achieved geological interpretation and with the aiming to of build-uping a new geological model of the study area (Fig. 7). These profiles cross ~~perpendicularly~~ the main structures perpendicularly to their strike and extend along the study area region from the northwest toward the southeast. This orientation allows to observe the structural relationships between Pesaro Anticline (PA) and Cornelia Anticline (CA) and their thrust faults, Pesaro Thrust (PT) and the

Cornelia Thrust (CT), providing a clearer view of the vertical and lateral distribution of the involved key stratigraphic units and of the tectonic features within the subsurface of the study area.

6.1. Multiple décollements and ~~En-en~~ echelon folds

595 In the area covered by this research, variations of mechanical anisotropy strongly influenced the structural setting, forming patterns of interconnected structures, detached along multiple décollements at different ~~depth~~ depths, corresponding to weak stratigraphic layers. Thus, the recognised tectonic structures have been grouped into two main categories: (i) deep-seated thrusts, represented by the innermost PT and the outermost CT (responsible for the formation of the large-wavelength structures PA and CA), which predominantly affect Mesozoic to Paleogene carbonate sequence; and (ii) shallow-seated thrusts, ~~which~~ ~~are~~ represented by closely spaced, short-wavelength structures of Tamara structure (TS), affecting ~~only a limited portion of the Upper Cretaceous and younger sequences, including the Oligocene, the the Miocene sequence and its the~~ overlying turbidite deposits. ~~Toward the front of the TS, these imbricated shallow-seated thrusts impact even shallower and younger sequences, involving only the Miocene and overlying turbidite deposits (Fig. 5a, 5b).~~ The depth converted profiles S1 and S2 ~~provides~~ ~~provide~~ a clear view of the spatial relationship among the aforementioned structures (Fig. 7a, 7b). PA is characterized by ~~a-an~~ NW-SE (along-strike) ~~extent of at least~~ ~ 30 km long and is ~ 12 km wide (along-dip, SW-NE direction, see profile S1 in Figs. 5a, 7a, 7d). Its wavelength (λ) as defined by Massoli et al. (2006), thus measured between the PA and CA crests, is ~11 km (Figs. 6a, 7b). ~~Section S1 shows PT being as~~ relatively flat in the shallow portion, ~~within the ~7-12 km distance range (~4 km), transitioning to a steeper ramp toward the southwest, whilst westward of its steeper ramp;~~ it is reasonable to image the PT lower décollement lying at around 9 km depth, possibly on top of the acoustic basement (~~base of the Triassic evaporites or top of the Permo-Triassic sequence; Mirabella et al., 2008; Barchi et al., 2012; Porreca et al., 2018~~). However, as profile S1 doesn't extend more to the south-western sector, the interpretation of the deepest structures is poorly constrained, ~~as thus~~ based on its interpreted trajectory. ~~Section S1 also shows a series of shallow imbricated, fore-verging and back-verging thrusts in the forelimb of the PA, forming TS, characterized by a length of ~10-20 km, a width of 7 km and a wavelength λ s of ~1.1 km (Figs. 5a, 5b, 7a, 7d). All these structures, including both fore-verging and back-verging thrusts, are associated to with the upper, décollement shallower semi-flat segment of the PT, which is extending detached at multiple stratigraphic levels. These detachments range from ~ 5 km depth within the Jurassic succession in the hanging wall of PT, to a sub-parallel/nearly parallel décollement within the Top Messinian (marly group), at roughly 3.5 km depth. The fore-verging imbricated thrusts originated originate from at different levels along this segment the upper décollement of the PT, ranging from upper Cretaceous (FUC) in the more internal imbricated thrust to the shallower levels within the weak, marly rocks (ranging from the upper Miocene to Pleistocene) Upper Miocene marly rocks in the more external imbricates toward the northeast. ; These thrusts propagates propagate both eastwards and upwards. This process resulted in multiple repetitions and duplications of the Miocene-Pliocene marly sequences. The nearby Tamara borehole further constraints our interpretation by drilling this shallower-shallowest décollement close to the base of the top Miocene "Marly Group" (Fig. 7a) and confirms the depth and the repetition of these~~

600

605

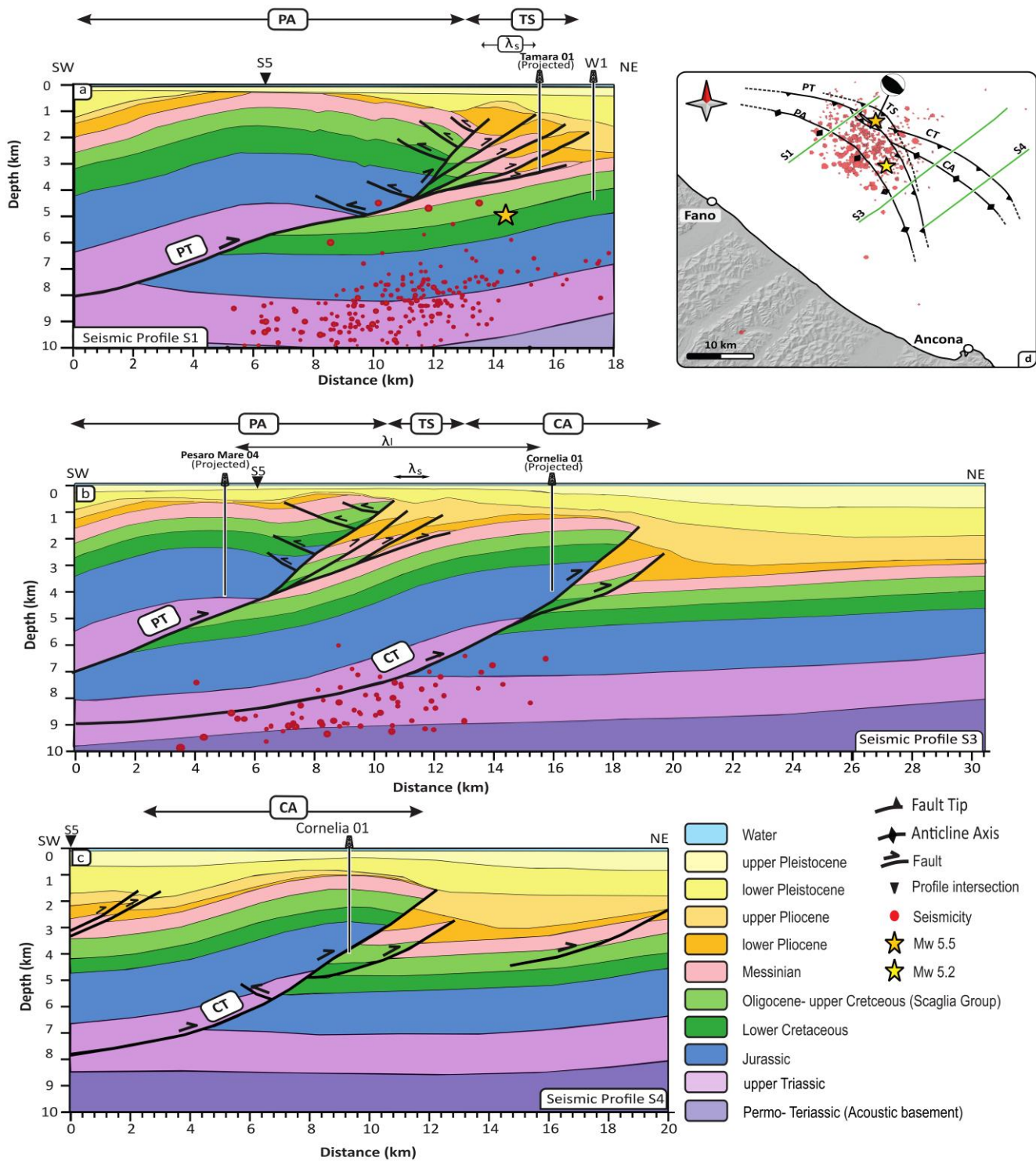
610

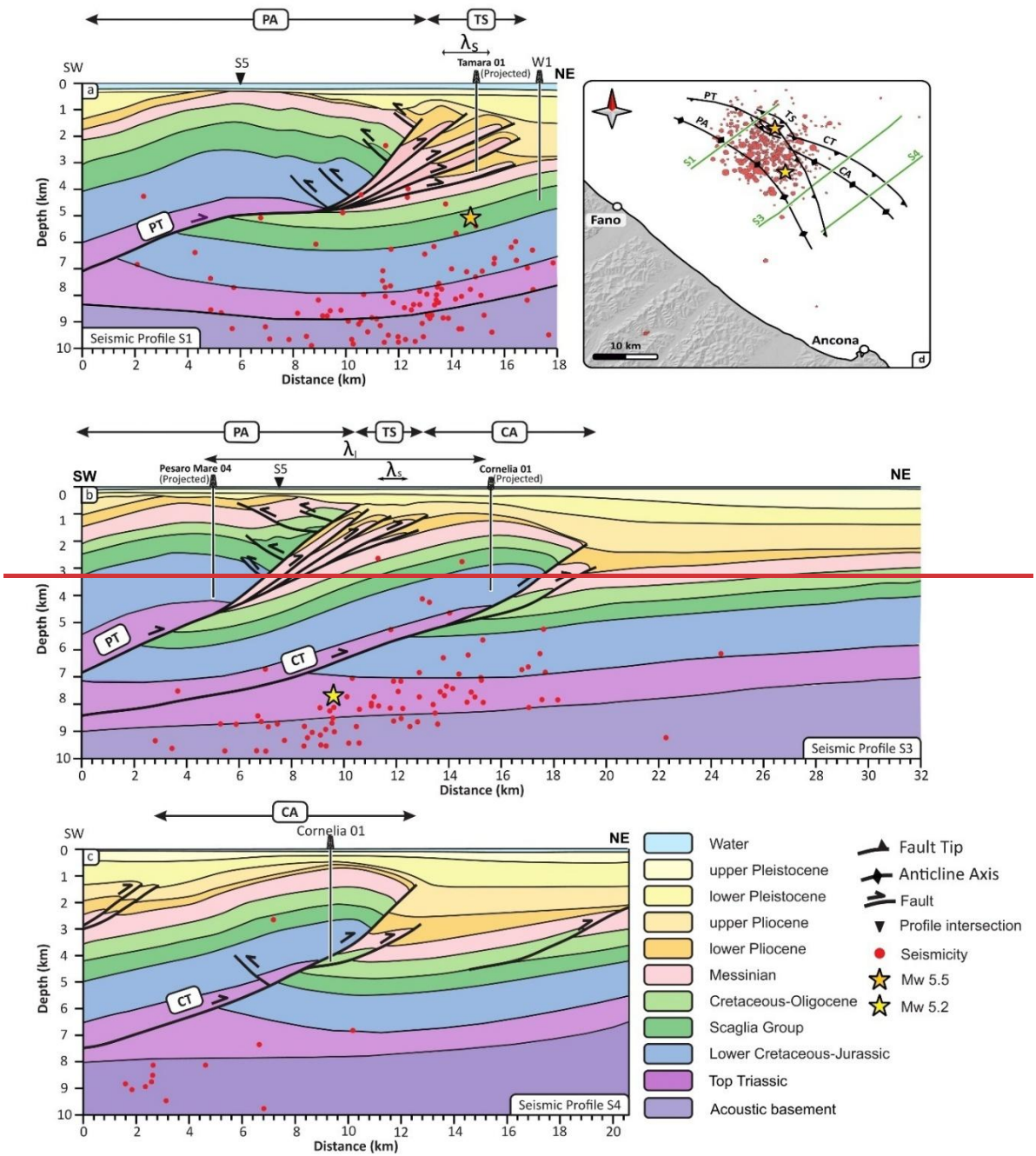
615

620

625 sequences across at least three slices. Since the Tamara well was drilled on the outermost part of the Tamara antiformal structure, it does not drill the complete series of imbricated thrusts and duplicated sedimentary sequences mapped in S1 (Figs. 5a,5b and 7a).

630 The overall analysis and observations of the seismic reflection profiles available on the southeasternmost extent of the study area, also allowed ~~to for the describe description of~~ the geometrical characteristics of CA, which are analogous to PA. It results in a NW-SE striking, ~ 20 km long (possibly extending just a few km further toward the SE) and ~ 12 km wide anticline (profile S4 in Figs. 6b, 7b, 7c) with a wavelength λ_1 of ~ 11 km (Figs. 6a, 7b). These structural wavelength values, λ_1 and λ_s , are larger than those obtained for corresponding structures in the Umbria-Marche area, where ~~corresponding structures have the~~ wavelengths wavelength range from 3.2 to 7.2 km for λ_1 and 0.4 to 2.3 km for λ_s (Massoli et al., 2006). These structures are ~~characterized~~ by lower syn-tectonic sedimentation. Conversely, the observed structural wavelength values are ~~and they are~~ smaller than those observed in the Po Plain, where higher syn-tectonic sedimentation contributes to even larger structural wavelengths, with λ_1 ranging from 15.8 to 33 km and λ_s from 4.5 to 8.2 km (Massoli et al., 2006). This observation is confirmed by the relationship described by Massoli et al. (2006), where variations in structural wavelength are linked to both the depth of the active décollement and the thickness of syn-tectonic sediments.





640

Fig. 7. Geological sections derived from: a) seismic profile S1, b) seismic profile S3, and c) seismic profile S4. The main shock of 5.5 ML and aftershocks are projected normal to perpendicularly to the section within buffers of 5-, 7-, and 10- km, respectively. d) Location map of the interpreted anticlines and thrust faults (this work); the seismicity distribution is sourced from terremoti.ingv.it. λ_l : Wavelength of the large structures; λ_s : Wavelength of the small structures.

645

Our comparative analysis of the PA and CA anticlines, and their related deep-seated thrust systems PT and CT, points out some structural similarities and ~~distinction~~differences. From the analysis of the profiles S3 and S4 (Fig. 7b, 7c), ~~looking at~~considering both ~~the geometry of the anticlines~~geometry and the ~~trajectories of the thrusts~~trajectories, a shared deep décollement level has been can be inferred suggested at it is clear how the thrusts share a common deep décollement level, at approximately 8–9 km depth, ~~(comparable to)~~consistent with results reported in nearby areas ~~provided by~~ (e.g., Pauselli et al., 2006; ~~or~~ Lavecchia et al., 2004, 2024). Furthermore, evidence indicates that the thrusting style in this area is a thin-skinned type of deformation, aligning with the observed décollement depth and suggesting tectonic processes that control syn-tectonic sedimentation and accommodate deformation within the overlying sedimentary cover, without involving the basement (Fig. 7). Our interpretation demonstrates that, unlike the PT, the CT lacks an upper shallower décollement. Instead, the ramp of the CT terminates blindly at a depth of 2 km within the base of the upper Pliocene turbiditic successions (Figs. 7b, 7c), and only one imbricated fore-verging thrust has been identified in S4. The latter is also constrained by the Cornelia borehole stratigraphy, evidencing a doubling of the ~~early~~Upper Cretaceous carbonate succession (~~Seaglia~~SCA group) over approximately 4–3 km between ~16–19 km distance in section S3 and about 4 km between ~ 8–12 km in section S4 (Fig. 7b, 7c).

660 Considering the deeper structures involving the carbonates, this study documents the structural transition between two main compressional structures: the PA (internal) and the CA (external) anticlines. In map view (Fig. 7d), these structures are linked to a pair of en-echelon, vicariant, coalescent thrusts, the northernmost PT and the southernmost CT. The interpretation of the seismic lines clearly highlighted that the transition from PT and CT occurs through an intermediate region, where both structures are present (Fig. 7d) and can be viewed as adjacent segments of the outermost thrust of the Northern Apennines.

665 Representative examples of coalescent anticlines extensively crop out also in the Umbria-Marche Apennines (Barchi et al., 1998; Scarsella 1941; Lavecchia, 1981; Lavecchia et al., 1988; Lavecchia et al., 2023), and such examples have been described worldwide since Dahlstrom (1970).

Our investigation shows that the shallow-seated TS structure can be traced only in the southeastern termination of the deep-seated PA up to seismic Profile S3, where both PA and TS overlap on the back limb of the CA (Fig. 7b). However, in the

670 southeastern part of our study area, as seen in seismic profile S4, the shallow-seated imbricated fore-verging thrusts and their related antiformal stacks (TS) are not observable (Fig. 7c). Our investigations indicate that the TS represents the deformed wedge of the frontal part of the PA structure, formed within the hanging wall zone of Pesaro, thus it cannot be considered originated by a single deep-seated structure such as PT or CT and neither a northwest-eastward continuation of the Cornelia thrust.

675 In slightly external sectors, with respect to our studied area, evidence of deep thrusts has been reported from the analysis of low-quality public profiles (Adriatic Arc Front, e.g., Bice thrust, Lavecchia et al., 2023). However, the present study suggests that the PT and associated imbricates did not extend more to the North-East. This consideration is also testified by the presence of a complete sedimentary succession (from Cretaceous carbonates to thick Quaternary sequences). Additionally, in the borehole W1 (drilled in the foreland of the PA), no thrust faults are reported and the Top Messinian reflection correlates well

680 with the corresponding identified erosional boundary. Evidence of deeper, external fronts were not found in the reviewed commercial seismic reflection profiles available across this study area, possibly falling besides the data quality at depth or outside the data coverage.

6.2. Seismotectonic implications

685 The mechanical stratigraphy reveals that both the deep-seated PT and CT ramps cut through the brittle carbonate multilayer, from 3 down to 9 km depth. This range coincides with the depths of most of the seismicity recorded during the Fano-Pesaro 2022 sequence (terremoti.ingv.it, Revida et al., 2022), suggesting that these thrusts may potentially serve as seismogenic structures (Fig.8a). Both PT and CT are southwest-dipping thrusts, with an interpreted dip angle of 30°–35°, compatible with the mainshocks-mainshock's focal mechanism (with strike 128°, dip 34° and rake 84°, terremoti.ingv.it).

690 Given their potential seismogenic role, the relationship between earthquake magnitude and subsurface rupture length for both the PT and CT was analysed using the Empirical relationships for the thrust faults regression diagrams (e.g. Wells and Coppersmith, 1994 and Leonard, 2014). Fault length directly influences the maximum possible displacement, and consequently, the potential maximum magnitude (Scholz, 2019). According to the findings of this analysis, the estimated sizes of the PT (~360 km²) and CT (~240 km²) suggest that they are capable of generating seismic events with magnitudes of up to Mw 6.8 and Mw 6.5, respectively. The observed fault lengths are substantial enough to account for both recent and historical seismic activity in the region.

700 However, determining the exact causative faults for the 2022 November 9th earthquakes remains challenging. It is important to highlight the spatial mismatch (Fig. 1), in terms of both location and depth distribution, among the literature interpreted faults and the hypocentral records (terremoti.ingv.it; Table 2) as shown in Figure 1 and Figure 8. Comparing the published earthquake locations and relatively shallow depths (~ 5 km) with our new-interpretation, seismicity is scarcely distributed across the Cornelia region (Fig. 8a, 8d). The first November 9th, 5.5 Mw main shock appears more closely associated to with the PT (extending more to the North-East), other than to the CT, the latter being less extended to the North West (Figs. 7d, 8a). The second November 9th mainshock and the aftershocks fall in between the area covered by the seismic profiles S1 and S3, in the interpreted transfer area between PT and CT. This-These events is-are close to the PT zone and somewhat far from the CT's main area but occurring at greater depth (~ 8 km) in the footwall of the PT (Figs. 1, Fig.-7d). However, it is known that both earthquake hypocentres location and the depth of the “not-relocated” seismicity lack in accuracy (±1 km depth error for the mainshock reported in the INGV catalogue), particularly in the offshore, due to the limited coverage of seismic stations. Recently, several authors has-have re-located/relocated the seismicity recorded during this 2022 sequence. Pezzo et al. (2023), An et al. (2024) and Costanzo (2024) used different relocation methods and methodological approaches, and a significant uncertainty in defining seismic event depth compared to the location is noticeable. The first relocation by Pezzo et al. (2023) shifted the main shock 1.5 km N-NW, increasing its depth to ~8 km, while aftershocks moved slightly NE and farther offshore (Fig.8b, 8d). The second relocation by An et al. (2024) shifted the main shock 5 km southward, thus closer to the shoreline, with a shallower depth, and relocated the aftershock cluster 6 km S-SE (Fig.8c, 8d). The study also reports error

estimations, with maximum values ranging from 0.8 to 3.6 km in all three directions. The spatial distribution of the original (INGV catalogue) and relocated aftershock events, in this area, is farther from the CT and more concentrated around the PT and the transfer zone between the PT and CT (Figs. 1, 4 and 7d).

Despite most of the considerations introduced above suggest the recent seismicity related more to PT other than CT (Maesano et al., 2023), this seismicity analysis and whole study underscores the complexity of determining whether the PT or CT served as a primary source of the 2022 seismic activity, or eventually if the latter might be associated to with a possible deeper thrust as proposed by other authors (e.g., T1 as supposed proposed b in Lavecchia et al., 2023). y Lavecchia et al., 2023). However, such a hypothetical possible causative deeper fault is not clearly imaged or visible at depth within our within available vintage seismic reflection data profiles, possibly due to the characterized by a lack of clear reflected signals from deeper reflectors, or just by very weak and poorly continuous reflective patterns embedded within a high level of random noise characterizing, typical of the legacy profiles (Ercoli et al., 2023) or due to thlack of reflected signals from deeper structures.

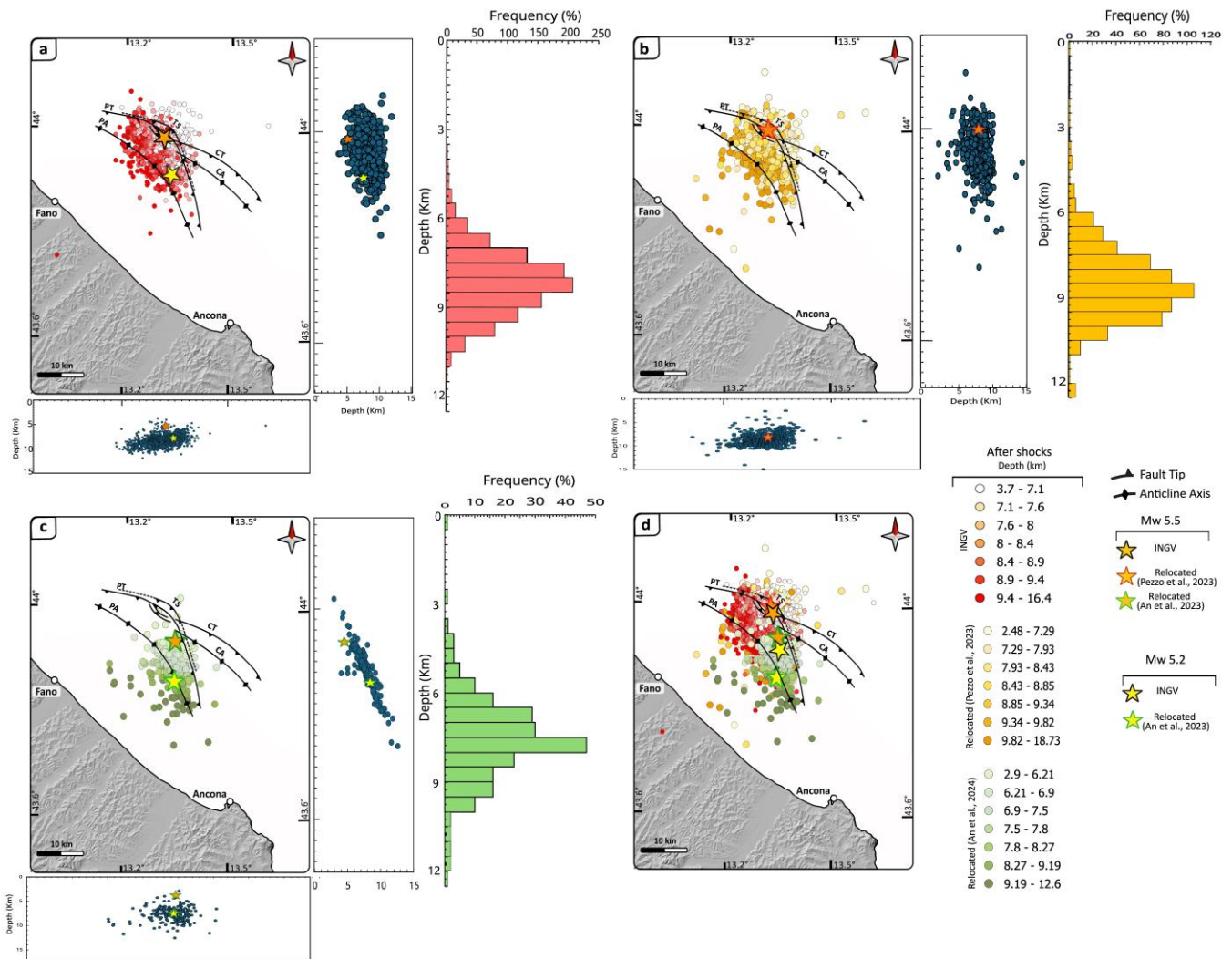


Fig.8. The spatial relationship between seismic events and the structural framework identified in this study, together with the depth distribution of seismicity shown through frequency histograms, seismic events are also projected on the latitude–depth and longitude–depth sections. The orange star marks the mainshock (Mw 5.5) and the yellow star the secondary shock (Mw 5.2) on 9 November 2022. a) Spatial distribution of the main shocks and aftershocks recorded by INGV between 1 November 2022 and 31 January 2023 (<https://terremoti.ingv.it/en>, accessed on 1 June 2025). b) Relocated seismicity from Pezzo et al. (2023) between 22 November 2022 and 5 January 2023, including the 9 November mainshock. c) Relocated seismicity from An et al., 2024 (200 seismic events) from 9 to 15 November 2022. d) Combined seismicity from INGV and relocated datasets.

Table 2. Location and depth parameters of the mainshocks for the 9th November 2022 Fano-Pesaro earthquake, as determined by different sources.

Event	Source	Depth (km)	Latitude	Longitude
-------	--------	------------	----------	-----------

Main Shock (Mw5.5)	INGV	5.0	43°58'59"N	13°19'26"E
	An et al., 2024	4.40	43°56'11"N	13°20'20"E
	Pezzo et al., 2023	7.94	43°59'41"N	13°18'58"E
Second Shock (Mw 5.2)	INGV	7.7	43°54'47.88"N	13°20'40.92"E
	An et al., 2024	8.4	43°51'36.36"N	13°20'16.44"E

The first relocation by Pezzo et al. (2023) shifted the main shock 1.5 km N NW, increasing its depth to 8 km, while aftershocks moved slightly NE and farther offshore. The second relocation by An et al. (2024) shifted the main shock 5 km southward, thus closer to the shoreline, with a shallower depth, and relocated the aftershock cluster 6 km S SE. The spatial distribution of the relocated aftershock events, as well as the historical seismicity in this area, is farther from the CT and more concentrated around the PT and the transfer zone between the PT and CT (Figs. 1 and 7d).

This analysis underscores the complexity of determining whether the PT or CT served as a primary source of the 2022 seismic activity or if the latter might be associated to a possible deeper thrust (e.g., T1 as supposed by Lavecchia et al., 2023). However, such a possible causative fault is not imaged at depth within our available seismic reflection data, possibly due to the high level of random noise characterizing the legacy profiles (Ereoli et al., 2023) or due to the lack of reflected signals from deeper structures.

5. Conclusions

This paper presents a new geological model of the tectonic structures of the Fano-Pesaro offshore area within the frontal part of the Northern Apennines. Multiple décollements located at different ~~depth depths~~ have been observed in the study area. These structures show a strong relationship between the depth of faulting and the wavelength of the related anticlines, influencing the kinematics of the thrust system. ~~This study suggests~~ the PT and CT ~~structures-thrusts~~ are ~~possibly~~ detached at depths of ~ 9 km on top of the acoustic basement. The two related PA and CA ~~structures-anticlines~~ can be followed along strike for about 50 km and are characterized by a wavelength in the order of ~ 11 km. The TS, ~~a series of imbricate thrusts,~~ develops along the shallow part of the ~~Pesaro thrust~~PT at a depth of 3.5 km, is characterized by a short wavelength (~ 1.1 km) of the imbricates spread along ~ 5 km in the forelimb of PA, and it can be followed ~~only~~ for ~10-20 km along strike. The PT and CT en-echelon arrangement, the presence of multiple detachments and the thin-skinned deformation (multiple décollements) suggest a geological model for this outermost sector of the Apennines, ~~thus~~ characterized by a thrust system not involving the ~~-acoustic~~ basement (thin-skinned tectonics).

This study highlights ~~a possible minor role of~~ the Cornelia thrust system ~~having a~~ during the 2022 earthquakes than previously ~~though~~ ~~thought~~ (Maesano et al., 2023). This is mainly due to ~~a more~~its limited extent toward the NW ~~as shown by our structural~~

~~interpretation. Although based on its geological, structural and geometrical characteristics this thrust system cannot be excluded as a seismogenic source, the~~. In addition, ~~t~~The ~~limited-spatial~~ distribution of ~~overal~~overall historical and recent seismicity ~~directly possibly affecting related with~~to the CT, ~~with its limited extension toward the north~~, is scarce and cannot be easily linked with it. ~~Although based on its geological, structural and geometrical characteristics, the is~~CT thrust system cannot be completely excluded as a seismogenic source, in the present study ~~T~~he ~~The~~ analysis and the integration of the relocated hypocentres ~~together with the~~and the new geological ~~model~~insights suggests that the PT, or a possible ~~easternmost~~deeper ~~easternmost~~ structure, would be ~~a~~ better ~~candidates~~candidate to be associated with the mainshocks. On the other hand, the relay zone between PT and CT is more coherent with the second main event. The still present uncertainty is mainly due to the low accuracy of the seismicity relocation caused by ~~the~~ lack of seismic stations ~~and simplified velocity models used~~. ~~On the light of all uncertainties related mainly to the inaccuracy of the offshore seismicity relocation and related depth estimation of the seismic events, it is therefore fundamental to provide solid geological constraints by relying on the unique subsurface data (seismic reflection and wells) available as well as on onshore analogues outcropping in the central Apennines~~. This work aims to remark that defining a solid subsurface geological model by integration of ~~these key data sources~~reflection seismic profiles ~~and boreholes data~~ (even if legacy) is essential in offshore areas. Building up a reliable, geologically driven model, allows ~~to~~ ~~refine~~for refining not only velocity models to use for more accurate earthquakes' relocation, but ~~also~~ for increasing the reliability of seismotectonic studies and ~~risks~~risk assessments. ~~The advancement of geological and geophysical studies might have broader benefits also on other application, such as supporting safer exploration projects of carbon capture and storage along the NA sea region~~. ~~On the light of all uncertainties related mainly to the inaccuracy of the offshore seismicity relocation and related depth estimation of the seismic events, it is therefore fundamental to provide solid geological constraints by relying on the unique subsurface data (seismic reflection and wells) available as well as on onshore analogues outcropping in the central Apennines (Massoli et al. 2006)~~.

Data availability

785 Supplementary data associated with this article can be found, in the online version

Author contribution

ES, ME, and MB contributed to the conception and design of the study. ES performed data curation, analysis, investigation, methodology, visualization, preparation of tables, maps and figures, and wrote the original draft of the manuscript. ME contributed to investigation, writing and revision. FC contributed to writing, revision, visualization maps and figures. FM and
790 AA contributed to the investigation, and revision. MB was responsible for conceptualization, resources, supervision, and review and editing. All authors contributed to the final revision of the manuscript and approved the version submitted.

Competing interests

The authors declare that they have no conflict of interest

795 **Acknowledgment:**

~~The authors express their gratitude to Schlumberger, Cegal, and PE Limited for providing academic licenses for their software platforms and plugins to the University of Perugia. These software and tools were used for uploading scanned legacy seismic profiles and well data (Blueback tools, Cegal), well digitization, and seismic interpretation with Petrel, as well as for structural modeling, and velocity model analysis with Petrel and Move. We also acknowledge the support teams of Petrel, Move, and Cegal for their prompt assistance in resolving technical challenges during the study. Additionally, we sincerely appreciate the QGIS and Inkscape Teams for developing free and open-source software, which was essential for data organization, correlation, and analysis (QGIS), as well as for image enhancement and digitization (Inkscape). We extend our special thanks to ENI for providing subsurface data under a confidential agreement, and to the Ministero dello Sviluppo Economico DGRME, the Società Geologica Italiana, Assomineraria, and CNR ViDEPI (<https://www.arcgis.com/>) for granting access to public domain data and services. We are also grateful to An and the Pezzo groups for sharing with us their catalogs of the relocated seismicity. We would like to sincerely thank the anonymous reviewers for their constructive comments and suggestions, which helped improve the quality of the manuscript. We are also deeply grateful to Professor Ramon Carbonell (Geo3BCN-CSIC, Spain) for his kind support and thoughtful feedback during the revision of the manuscript. The authors express their gratitude to Schlumberger, Cegal, and PE Limited for providing academic licenses for their software platforms and plugins to the University of Perugia. These software and tools were used for uploading scanned legacy seismic profiles and well data (Blueback tools, Cegal), well digitization, and seismic interpretation with Petrel, as well as for structural modeling, and velocity model analysis with Petrel and Move. We also acknowledge the support teams of Petrel, Move, and Cegal for their prompt assistance in resolving technical challenges during the study. Additionally, we sincerely appreciate the QGIS and Inkscape Teams for developing free and open-source software, which was essential for data organization, correlation, and analysis (QGIS), as well as for image enhancement and digitization (Inkscape). We extend our special thanks to ENI for providing subsurface data under a confidential agreement, and to the Ministero dello Sviluppo Economico DGRME, the Società Geologica Italiana, Assomineraria, and CNR ViDEPI (<https://www.arcgis.com/>) for granting access to public domain data and services. We are also grateful to An and the Pezzo groups for sharing with us their catalogs of the relocated seismicity.~~

References

- 820 Alvarez, W., 1999. Drainage on evolving fold-thrust belts: a study of transverse canyons in the Apennines. *Basin Research* 11, 267–284.
- Amadori, C., Toscani, G., Di Giulio, A., Maesano, F.E., D’Ambrogio, C., Ghielmi, M. and Fantoni, R., 2019. From cylindrical to non-cylindrical foreland basin: Pliocene–Pleistocene evolution of the Po Plain–Northern Adriatic basin (Italy). *Basin Research*, 31(5), pp.991-1015. <https://doi.org/10.1111/bre.12369>.
- 825 Amadori, C., Ghielmi, M., Mancin, N. and Toscani, G., 2020. The evolution of a coastal wedge in response to Plio-Pleistocene climate change: The Northern Adriatic case. *Marine and Petroleum Geology*, 122, p.104675. <https://doi.org/10.1016/j.marpetgeo.2020.104675>.
- An, L., Grigoli, F., Enescu, B., Buttinelli, M., Anselmi, M., Molinari, I. and Ito, Y., 2024. Offshore Fault Geometry Revealed from Earthquake Locations Using New State-of-Art Techniques: The Case of the 2022 Adriatic Sea Earthquake
- 830 Sequence. *Seismological Research Letters*, 95(5), pp.2779-2790. <https://doi.org/10.1785/0220230264>.
- Argnani, A., 1998. Structural elements of the Adriatic foreland and their relationships with the front of the Apennine fold-and-thrust belt. *Memorie della Societa Geologica Italiana*, 52, 647–654.
- Bally, A.W., 1986. Balanced sections and seismic reflection profiles across the Central Apennines. *Mem. Soc. Geol. It.*, 35, pp.257-310.
- 835 Barbieri, C., Di Giulio, A., Massari, F., Asioli, A., Bonato, M. and Mancin, N., 2007. Natural subsidence of the Venice area during the last 60 Myr. *Basin Research*, 19(1), pp.105-123. <https://doi.org/10.1111/j.1365-2117.2007.00314.x>
- Barchi M.R., De Feyter A., Magnani M.B., Minelli G., Pialli G. & Sotera B.M. (1998) - The structural style of the Umbria-Marche fold and thrust belt. *Mem. Soc. Geol. It.* 52, 557-578.
- Barchi M.R., 2010. The Neogene-Quaternary evolution of the Northern Apennines: crustal structure, style of deformation
- 840 and seismicity. In: (Eds.) Beltrando M., Peccerillo A., Mattei M., Conticelli S., and Doglioni C., *Journal of the Virtual Explorer*, volume 36, paper 10, doi: 10.3809/jvirtex.2009.00220.
- Barchi, M.R., Alvarez, W. and Shimabukuro, D.H., 2012. The Umbria-Marche Apennines as a double orogen: observations and hypotheses. *Italian Journal of Geosciences*, 131(2), pp.258-271. <https://doi.org/10.3301/IJG.2012.17>
- Barchi, M.R., Carboni, F., Michele, M., Ercoli, M., Giorgetti, C., Porreca, M., Azzaro, S. and Chiaraluce, L., 2021. The
- 845 influence of subsurface geology on the distribution of earthquakes during the 2016–2017 Central Italy seismic sequence. *Tectonophysics*, 807, p.228797. <https://doi.org/10.1016/j.tecto.2021.228797>.
- [*Bencini, R., & Martinuzzi, A., 2012. Relazione Tecnica Geologica – Studio di Impatto Ambientale – Istanza di licenza di esplorazione per lo stoccaggio geologico di biossido di carbonio denominata “Sibilla”. Technical Report, Independent Gas Management S.r.l. DOI: 10.13140/RG.2.2.28746.16327*](#)
- 850 Berberian, M., 1995. Master “blind” thrust faults hidden under the Zagros folds: active basement tectonics and surface morphotectonics. *Tectonophysics* 241, 193–224. [https://doi.org/10.1016/0040-1951\(94\)00185-C](https://doi.org/10.1016/0040-1951(94)00185-C).

- Bigi, G., Cosentino, D., Parotto, M., Sartori, R., & Scandone, P., 1992. Structural model of Italy and gravity map, 1:500,000. S.EL.CA.
- Bianco, E., 2014. Geophysical tutorial: Well-tie calculus. *The Leading Edge*, 33(6), pp.674-677.
- 855 Billi, A., 2005. Attributes and influence on fluid flow of fractures in foreland carbonates of southern Italy. *Journal of Structural Geology*. 27, 1630-1643.
- Brancolini, G., Civile, D., Donda, F., Tosi, L., Zecchin, M., Volpi, V., Rossi, G., Sandron, D., Ferrante, G.M., Forlin, E., 2019. New insights on the Adria plate geodynamics from the northern Adriatic perspective. *Mar. Petrol. Geol.* 109, 687–697.
- 860 Bonini, L., Toscani, G. and Seno, S., 2014. Three-dimensional segmentation and different rupture behavior during the 2012 Emilia seismic sequence (Northern Italy). *Tectonophysics*, 630, pp.33-42.
- Boschi E., Guidoboni E., Ferrari G., Mariotti D., Valensise G., Gasperini P. (eds), 2000. Catalogue of Strong Italian Earthquakes from 461 B.C. to 1997. *Annali di Geofisica*, 43, 4, 609-868.
- 865 Burrato, P., Vannoli, P., Fracassi, U., Basili, R. and Valensise, G., 2012. Is blind faulting truly invisible? Tectonic-controlled drainage evolution in the epicentral area of the May 2012, Emilia-Romagna earthquake sequence (northern Italy). *Annals of Geophysics*.
- Carboni, F., Brozzetti, F., Mirabella, F., Cruciani, F., Porreca, M., Ercoli, M., Back, S., Barchi, M.R., 2020a. Geological and geophysical study of a thin-skinned tectonic wedge formed during an early collisional stage: the Trasimeno Tectonic Wedge (Northern Apennines, Italy). *Geol. Mag.* 157 (2), 213–232. <https://doi.org/10.1017/S001675681900061X>.
- 870 Carboni, F., Viola, G., Aldega, L., Van der Leji, R., Brozzetti, F., Barchi, M.R., 2020b. K-Ar fault gouge dating of Neogene thrusting: the case of the siliciclastic deposits of the Trasimeno Tectonic Wedge (Northern Apennines, Italy). *Ital. J. Geosci.* 139 (2), 300–308. <https://doi.org/10.3301/IJG.2020.06>.
- Carboni, F., Mirabella, F., Minelli, G., Saleh, H., Porreca, M., Ercoli, M., Pauselli, C. and Barchi, M.R., 2024. Kinematic reconstruction of active tectonic and halokinetic structures in the 2021 NW Palagruža earthquake area (Central Adriatic). *Journal of Structural Geology*, 182, p.105112.
- 875 Caricchi, C., Cifelli, F., Sagnotti, L., Sani, F., Speranza, F. and Mattei, M., 2014. Paleomagnetic evidence for a post-Eocene 90° CCW rotation of internal Apennine units: A linkage with Corsica-Sardinia rotation. *Tectonics*, 33(4), pp.374-392.
- Carminati, E., Corda, L., Mariotti, G., Scifoni, A. and Trippetta, F., 2013. Mesozoic syn- and postdrift evolution of the central Apennines, Italy: the role of triassic evaporites. *The Journal of Geology*, 121(4), pp.327-354.
- 880 Casero, P. and Bigi, S., 2013. Structural setting of the Adriatic basin and the main related petroleum exploration plays. *Marine and Petroleum Geology*, 42, pp.135-147.
- Castellarin, A., Eva, C., Giglia, G., Vai, G.B., Rabbi, E., Pini, G.A. and Crestana, G., 1985. Analisi strutturale del fronte appenninico padano. *Giornale di Geologia*, 47(1-2), pp.47-75.

- Centamore, E., Adamoli, L., Berti, D., Bigi, G., Bigi, S., Casnedi, R., Cantalamessa, G., Fumanti, F., Morelli, C., Micarelli, A. and Ridolfi, M., 1992. Carta geologica dei bacini della Lagaffe del Cellino e dei rilievi carbonatici circostanti. Studi Geologici Camerti, Vol. Spec.
- Channell, J.E., d'Argenio, B. and Horvath, F., 1979. Adria, the African promontory, in Mesozoic Mediterranean palaeogeography. *Earth-Science Reviews*, 15(3), pp.213-292.
- Chiaraluce, L., Barchi, M.R., Carannante, S., Collettini, C., Mirabella, F., Pauselli, C. and Valoroso, L., 2017. The role of rheology, crustal structures and lithology in the seismicity distribution of the northern Apennines. *Tectonophysics*, 694, pp.280-291.
- Ciaccio, M.G., Barchi, M.R., Chiarabba, C., Mirabella, F. and Stucchi, E., 2005. Seismological, geological and geophysical constraints for the Gualdo Tadino fault, Umbria–Marche Apennines (central Italy). *Tectonophysics*, 406(3-4), pp.233-247.
- Costanzo, A., 2024. A New Catalogue and Insights into the 2022 Adriatic Offshore Seismic Sequence Using a Machine Learning-Based Procedure. *Sensors*, 25(1), p.82.
- Cuffaro, M., Riguzzi, F., Scrocca, D., Antonioli, F., Carminati, E., Livani, M. and Doglioni, C., 2010. On the geodynamics of the northern Adriatic plate. *Rendiconti Lincei*, 21, pp.253-279.
- Dahlstrom, C.D., 1970. Structural geology in the eastern margin of the Canadian Rocky Mountains. *Bulletin of Canadian Petroleum Geology*, 18(3), pp.332-406.
- D'agostino, N., Avallone, A., Cheloni, D., D'anastasio, E., Mantenuto, S. and Selvaggi, G., 2008. Active tectonics of the Adriatic region from GPS and earthquake slip vectors. *Journal of Geophysical Research: Solid Earth*, 113(B12).
- De Feyter, A.J., Koopman, A., Molenaar, N., Ende, C.V.D., 1986. Detachment tectonics and sedimentation, Umbro-Marchean Apennines, (Italy). *Bollettino della Società Geologica Italiana* 105, 65–85.
- De Feyter, A.J., 1991. *Gravity tectonics and sedimentation of the Montefeltro, Italy* (No. 35). Faculteit Aardwetenschappen der Rijksuniversiteit te Utrecht.
- De Nardis, R., Pandolfi, C., Cattaneo, M., Monachesi, G., Cirillo, D., Ferrarini, F., Bello, S., Brozzetti, F. and Lavecchia, G., 2022. Lithospheric double shear zone unveiled by microseismicity in a region of slow deformation. *Scientific Reports*, 12(1), p.21066.
- Déverchère, J., Yelles, K., Domzig, A., Mercier de Lépinay, B., Bouillin, J.P., Gaullier, V., Bracène, R., Calais, E., Savoye, B., Kherroubi, A. and Le Roy, P., 2005. Active thrust faulting offshore Boumerdes, Algeria, and its relations to the 2003 Mw 6.9 earthquake. *Geophysical research letters*, 32(4).
- Dewey, J.F., Helman, M.L., Knott, S.D., Turco, E. and Hutton, D.H.W., 1989. Kinematics of the western Mediterranean. Geological Society, London, Special Publications, 45(1), pp.265-283.
- Di Bucci, D., Mazzoli, S., 2002. Active tectonics of the Northern Apennines and Adria geodynamics: new data and a discussion. *Journal of Geodynamics*, 34, Issue 5, 687-707. [https://doi.org/10.1016/S0264-3707\(02\)00107-2](https://doi.org/10.1016/S0264-3707(02)00107-2).

- DISS Working Group (2021). Database of Individual Seismogenic Sources (DISS), Version 3.3.0: A compilation of potential sources for earthquakes larger than M 5.5 in Italy and surrounding areas. Istituto Nazionale di Geofisica e Vulcanologia (INGV). <https://doi.org/10.13127/diss3.3.0>.
- 920 Ercoli, M., Carboni, F., Akimbekova, A., Carbonell, R.B. and Barchi, M.R., 2023. Evidencing subtle faults in deep seismic reflection profiles: Data pre-conditioning and seismic attribute analysis of the legacy CROP-04 profile. *Frontiers in Earth Science*, 11, p.1119554.
- Fantoni, R. & Franciosi, R., 2010. Tectono-sedimentary setting of the Po Plain and Adriatic foreland. *Rendiconti Lincei*. 21, 197–209.
- 925 Finetti, I.R., Del Ben, A., 2005. Crustal Tectono-Stratigraphic Setting of the Adriatic Sea from New CROP Seismic Data. CROP PROJECT: Deep. Elsevier, pp. 519–547 (Chapter 23)
- Franklin D. Wolfe, John H. Shaw, Andreas Plesch, Daniel J. Ponti, James F. Dolan, Mark R. Legg; The Wilmington Blind-Thrust Fault: An Active Concealed Earthquake Source beneath Los Angeles, California. *Bulletin of the Seismological Society of America* 2019; 109 (5): 1890–1906. doi: <https://doi.org/10.1785/0120180335>.
- 930 Frignani, M. and Langone, L., 1991. Accumulation rates and ^{137}Cs distribution in sediments off the Po River delta and the Emilia-Romagna coast (northwestern Adriatic Sea, Italy). *Continental Shelf Research*, 11(6), pp.525-542.
- Geletti, R., Del Ben, A., Busetti, M., Ramella, R. and Volpi, V. (2008), Gas seeps linked to salt structures in the Central Adriatic Sea. *Basin Research*, 20: 473-487. <https://doi.org/10.1111/j.1365-2117.2008.00373.x>.
- 935 Ghielmi, M., Minervini, M., Nini, C., Rogledi, S., Rossi, M., 2010a. Sedimentary and tectonic evolution in the eastern Po Plain and northern Adriatic Sea area from Messinian to Middle Pleistocene (Italy). In: Sassi, F.P. (Ed.), *Nature and Geodynamics of the Lithosphere in Northern Adriatic*. *Rend. Fis. Acc. Lincei*, 21 (Suppl.1), pp. 131e166. <http://dx.doi.org/10.1007/s12210-010-0101-5>.
- Ghielmi, M., Minervini, M., Nini, C., Rogledi, S. and Rossi, M., 2013. Late Miocene–Middle Pleistocene sequences in the Po Plain–Northern Adriatic Sea (Italy): the stratigraphic record of modification phases affecting a complex foreland basin. *Marine and Petroleum Geology*, 42, pp.50-81.
- 940 Guidoboni, E., Ferrari, G., Tarabusi, G., Sgattoni, G., Comastri, A., Mariotti, D., Ciuccarelli, C., Bianchi, M.G. and Valensise, G., 2019. CFTI5Med, the new release of the catalogue of strong earthquakes in Italy and in the Mediterranean area. *Scientific Data*, 6(1), p.80.
- Gunderson, K. L., Anastasio, D. J., Pazzaglia, F. J., and Picotti, V. (2013). Fault slip rate variability on 104-105yr timescales for the Salsomaggiore blind thrust fault, Northern Apennines, Italy. *Tectonophysics* 608, 356–365. doi: 10.1016/j.tecto.2013.09.018.
- 945 Gunderson, K.L., Anastasio, D.J., Pazzaglia, F.J. and Kodama, K.P., 2018. Intrinsically variable blind thrust faulting. *Tectonics*, 37(5), pp.1454-1471

- Handy, M. R., Ustaszewski, K., & Kissling, E., 2015. Reconstructing the Alps–Carpathians–Dinarides as a key to understanding switches in subduction polarity, slab gaps and surface motion. *International Journal of Earth Sciences*, 104(1), 1–26. <https://doi.org/10.1007/s00531-014-1060-3>.
- Hayes, G.P., Briggs, R.W., Sladen, A., Fielding, E.J., Prentice, C., Hudnut, K., Mann, P., Taylor, F.W., Crone, A.J., Gold, R. and Ito, T., 2010. Complex rupture during the 12 January 2010 Haiti earthquake. *Nature Geoscience*, 3(11), pp.800-805.
- Van Hinsbergen, D.J., Torsvik, T.H., Schmid, S.M., Mañenco, L.C., Maffione, M., Vissers, R.L., Gürer, D. and Spakman, W., 2020. Orogenic architecture of the Mediterranean region and kinematic reconstruction of its tectonic evolution since the Triassic. *Gondwana Research*, 81, pp.79-229.
- Koopman, A., 1983. Detachment tectonics in the central Apennines, Italy (Doctoral dissertation, Instituut voor Aardwetenschappen der Rijksuniversiteit te Utrecht).
- Latorre, D., Mirabella, F., Chiaraluce, L., Trippetta, F. and Lomax, A., 2016. Assessment of earthquake locations in 3-D deterministic velocity models: A case study from the Altotiberina Near Fault Observatory (Italy). *Journal of Geophysical Research: Solid Earth*, 121(11), pp.8113-8135.
- Lavecchia, G., 1981. Appunti per uno schema strutturale dell'Appennino Umbro-Marchigiano. III: Lo stile deformativo.
- Lavecchia, G., Minelli, G. and Pialli, G., 1988. The Umbria-Marche arcuate fold belt (Italy). *Tectonophysics*, 146(1-4), pp.125-137.
- Lavecchia, G., Boncio, P., Creati, N., Brozzetti, F., 2004. Stile strutturale, stato termico-meccanico e significato sismogenetico del thrust Adriatico: dati e spunti da una revisione del profilo CROP 03 integrata con l'analisi di dati sismologici. *Bollettino della Societa` Geologica Italiana* 123, 111–125.
- Lavecchia, G., Pietrolungo, F., Bello, S., Talone, D., Pandolfi, C., Andrenacci, C., Carducci, A. and de Nardis, R., 2023. Slowly Deforming Megathrusts within the Continental Lithosphere: A Case from Italy. *GSA TODAY*, 34(1), pp.4-10.
- Leonard, M., 2014. Self-consistent earthquake fault-scaling relations: Update and extension to stable continental strike-slip faults. *Bulletin of the Seismological Society of America*, 104(6), pp.2953-2965.
- Lettis, W.R., Wells, D.L. and Baldwin, J.N., 1997. Empirical observations regarding reverse earthquakes, blind thrust faults, and quaternary deformation: Are blind-thrust faults truly blind? *Bulletin of the Seismological Society of America*, 87(5), pp.1171-1198.
- Livani, M., Scrocca, D., Arecco, P. and Doglioni, C., 2018. Structural and stratigraphic control on salient and recess development along a thrust belt front: The Northern Apennines (Po Plain, Italy). *Journal of Geophysical Research: Solid Earth*, 123(5), pp.4360-4387.
- Locati M., Camassi R., Rovida A., Ercolani E., Bernardini F., Castelli V., Caracciolo C.H., Tertulliani A., Rossi A., Azzaro R., D'Amico S., Antonucci A., 2022. Database Macrosismico Italiano (DBMI15), versione 4.0 [Data set]. Istituto Nazionale di Geofisica e Vulcanologia (INGV). <https://doi.org/10.13127/dbmi/dbmi15.4>

- 980 Ioualalen, Bernard Pelletier, Gabriela Solis Gordillo, Investigating the March 28th 1875 and the September 20th 1920 earthquakes/tsunamis of the Southern Vanuatu arc, offshore Loyalty Islands, New Caledonia, *Tectonophysics*, Volume 709, 2017, Pages 20-38, ISSN 0040-1951, <https://doi.org/10.1016/j.tecto.2017.05.006>
- Maesano, F. E., Toscani, G., Burrato, P., Mirabella, F., D'Ambrogi, C., and Basili, R., 2013. Deriving thrust fault slip rates from geological modeling: Examples from the Marche coastal and offshore contraction belt, Northern Apennines, Italy. *Mar. Petrol. Geol.* 42, 122–134. doi: 10.1016/j.marpetgeo.2012.10.008.
- 985 Maesano, F. E., D'Ambrogi, C., Burrato, P., & Toscani, G., 2015. Slip-rates of blind thrusts in slow deforming areas: examples from the Po Plain (Italy). *Tectonophysics*, 643, 8-25.
- Latorre, D., Mirabella, F., Chiaraluce, L., Trippetta, F., Lomax, A., 2016. Assessment of earthquake locations in 3-D deterministic velocity models: A case study from the Altotiberina Near Fault Observatory (Italy): Event Locations in
990 Deterministic Models. *Journal of Geophysical Research: Solid Earth* 121, 8113–8135. <https://doi.org/10.1002/2016JB013170>
- Maesano, F. E., & D'Ambrogi, C., 2016. Coupling sedimentation and tectonic control: Pleistocene evolution of the central Po Basin. *Italian Journal of Geosciences*, 135(3), 394-407.
- Maesano, F. E., Buttinelli, M., Maffucci, R., Toscani, G., Basili, R., Bonini, L., et al., 2023. Buried alive: Imaging the 9
995 November 2022, Mw 5.5 earthquake source on the offshore Adriatic blind thrust front of the Northern Apennines (Italy). *Geophysical Research Letters*, 50, e2022GL102299. <https://doi.org/10.1029/2022GL102299>.
- Mantovani, E., Babbucci, D., Viti, M., Albarello, D., Mugnaioli, E., Cenni, N., et al., 2006. Post-Late Miocene kinematics of the Adria microplate: inferences from geological, geophysical and geodetic data, in *The Adria Microplate: GPS Geodesy, Tectonics and Hazards. Nato Science Series: IV: Earth and Environmental Sciences*, 61, 51–69. doi: 10.1007/1-4020-4235-3_04.
1000
- Maramai, A., Brizuela, B. and Graziani, L., 2022. A Database for Tsunamis and Meteotsunamis in the Adriatic Sea. *Applied Sciences*, 12(11), p.5577.
- Massoli, D., Koyi, H.A. and Barchi, M.R., 2006. Structural evolution of a fold and thrust belt generated by multiple décollements: analogue models and natural examples from the Northern Apennines (Italy). *Journal of Structural Geology*,
1005 28(2), pp.185-199.
- Mattavelli, L., Novelli, L. & Anelli, L., 1991. Occurrence of hydrocarbons in the Adriatic basin. *Spec. Publ. EAPG*, 1, 369-380.
- Mazzanti, R. and Trevisan, L., 1978. Evoluzione della rete idrografica nell'Appennino centro-settentrionale. *Geografia Fisica e Dinamica Quaternaria*, 1(1), pp.55-62.
- 1010 Mazzoli, S., Santini, S., Macchiavelli, C., & Ascione, A., 2015. Active tectonics of the outer northern Apennines: Adriatic vs. Po Plain seismicity and stress fields. *Journal of Geodynamics*, 84, 62–76. <https://doi.org/10.1016/j.jog.2014.10.northern.002>.
- Menichetti, M. and Coccioni, R., 2013. Umbria-Marche Apennines geological field trip.

- 1015 Mirabella, F, Ciaccio M.G., Barchi M.R., Merlini S., 2004. The Gubbio normal fault (Central Italy): geometry, displacement distribution and tectonic evolution, *Journal of Structural Geology*. 26, 2233-2249, ISSN 0191-8141, <https://doi.org/10.1016/j.jsg.2004.06.009>.
- Mirabella, F., Barchi, M. R., & Lupattelli, A., 2008. Seismic reflection data in the Umbria Marche region: Limits and capabilities to unravel the subsurface structure in a seismically active area. *Annals of Geophysics*, 51(2–3), 383–396. <https://doi.org/10.4401/ag-3032>.
- 1020 Molli, G., 2008. Northern Apennine–Corsica orogenic system: an updated overview (Vol. 298, No. 1, pp. 413-442). London: The Geological Society of London.
- Molli, G. and Malavieille, J., 2011. Introduction to the Field trips of the CorseAlp 2011. *Journal of the Virtual Explorer*, 39, pp.paper-1.
- 1025 Montone, P. and Mariucci, M.T., 2023. Deep well new data in the area of the 2022 Mw 5.5 earthquake, Adriatic Sea, Italy: In situ stress state and P-velocities. *Frontiers in Earth Science*, 11, p.1164929.
- [Murgia, M. V., Ronchi P., Ceriani A., 2004. Dolomitization processes and their relationships with the evolution of an orogenic belt \(central Apennines and peri-Adriatic foreland, Italy\), in R. Swennen, F. Roure, and J. W. Granath, eds., Deformation, fluid flow, and reservoir appraisal in foreland fold and thrust belts: AAPG Hedberg Series, no. 1, p. 277–294.](#)
- 1030 Nespoli, M., Belardinelli, M.E., Gualandi, A., Serpelloni, E. and Bonafede, M., 2018. Poroelasticity and fluid flow modeling for the 2012 Emilia-Romagna earthquakes: Hints from GPS and InSAR data. *Geofluids*, 2018(1), p.4160570.
- Ollier, C.D. and Pain, C.F., 2009. The Apennines, the Dinarides, and the Adriatic Sea: is the Adriatic Microplate a reality?. *Geografia Fisica e Dinamica Quaternaria*, 32(2), pp.167-175.
- 1035 Palano, M., Pezzo, G., Serpelloni, E., Devoti, R., D’Agostino, N., Gandolfi, S., Sparacino, F., Anderlini, L., Poluzzi, L., Tavasci, L. and Macini, P., 2020. Geopositioning time series from offshore platforms in the Adriatic Sea. *Scientific Data*, 7(1), p.373.
- Panara Y, Maesano FE, Amadori C, Fedorik J, Toscani G and Basili R.,2021. Probabilistic Assessment of Slip Rates and Their Variability Over Time of Offshore Buried Thrusts: A Case Study in the Northern Adriatic Sea. *Front. Earth Sci.* 9:664288. doi: 10.3389/feart.2021.664288.
- 1040 Pandolfi, C., Taroni, M., de Nardis, R., Lavecchia, G. and Akinci, A., 2024. Advanced 3D seismic hazard analysis for active compression in the Adriatic Thrust Zone, Italy. *Bulletin of Earthquake Engineering*, pp.1-24.
- Pauselli, C., Marchesi, R. and Barchi, M.R., 2002. Seismic image of the compressional and extensional structures in the Gubbio area (Umbrian-Pre Apennines). *BOLLETTINO DELLA SOCIETÀ GEOLOGICA ITALIANA. VOLUME SPECIALE*, pp.263-272.
- 1045 Pauselli, C., Barchi, M.R., Federico, C., Magnani, M.B. and Minelli, G., 2006. The crustal structure of the Northern Apennines (Central Italy): an insight by the CROP03 seismic line. *American Journal of Science*, 306(6), pp.428-450.

- Pezzo, G., Merryman Boncori, J.P., Tolomei, C., Salvi, S., Atzori, S., Antonioli, A., Trasatti, E., Novali, F., Serpelloni, E., Candela, L. and Giuliani, R., 2013. Coseismic deformation and source modeling of the May 2012 Emilia (Northern Italy) earthquakes. *Seismological Research Letters*, 84(4), pp.645-655.
- 1050 Pezzo, G., Petracchini, L., Devoti, R., Maffucci, R., Anderlini, L., Antonucci, I., et al., 2020. Active fold-thrust belt to foreland transition in northern Adria, Italy, tracked by seismic reflection profiles and GPS offshore data. *Tectonics*, 39, e2020TC006425. <https://doi.org/10.1029/2020TC006425> Received 9 JUL 2020 Accepted 7 OCT 2020 Accepted article online 9 NOV 2020 PEZZO ET AL. 1 of 21
- 1055 Pezzo, G., Billi, A., Carminati, E. et al., 2023. Seismic source identification of the 9 November 2022 Mw 5.5 offshore Adriatic Sea (Italy) earthquake from GNSS data and aftershock relocation. *Sci Rep* 13, 11474. <https://doi.org/10.1038/s41598-023-38150-5>.
- Piccardi, L., Sani, F., Moratti, G., Cunningham, D. and Vittori, E., 2011. Present-day geodynamics of the circum-Adriatic region: An overview. *Journal of geodynamics*, 51(2-3), pp.81-89.
- Pieri, M. and Groppi, G., 1981. Subsurface geological structure of the Po Plain, Italy. Verlag nicht ermittelbar.
- 1060 Porreca, M., Minelli, G., Ercoli, M., Brobia, A., Mancinelli, P., Cruciani, F., et al (2018). Seismic reflection profiles and subsurface geology of the area interested by the 2016–2017 earthquake sequence (Central Italy). *Tectonics*, 37, 1116–1137. <https://doi.org/10.1002/2017TC004915>.
- Ricci Lucchi, F., 1986. The Oligocene to Recent foreland basins of the northern Apennines. *Foreland basins*, pp.103-139.
- 1065 Roering, J., Cooke, M.L., Pollard, D., 1997. Why blind thrust faults do not propagate to the Earth's surface: numerical modeling of coseismic deformation associated with thrust-related anticlines. *J. Geophys. Res.* 102, 11901–11912.
- Rovida, A., Locati, M., Camassi, R., Lolli, B., Gasperini, P., & Antonucci, A. (2022). *Catalogo Parametrico dei Terremoti Italiani (CPTI15)*, versione 4.0 [Dataset]. Istituto Nazionale di Geofisica e Vulcanologia (INGV). <https://doi.org/10.13127/CPTI/CPTI15.4>.
- 1070 [Ronchi, P., Casaglia, F., Ceriani, A., 2003. -The Multiphase Dolomitization of the Liassic Calcare Massiccio and Corniola \(Montagna dei Fiori, Northern Apennines, Italy\). *Boll. Soc. Geol. It.*, 122, 157-172.](#)
- Sani, F., Vannucci, G., Boccaletti, M., Bonini, M., Corti, G. and Serpelloni, E., 2016. Insights into the fragmentation of the Adria Plate. *Journal of Geodynamics*, 102, pp.121-138.
- [Scarsella, F. \(1941\). Carta geologica d'Italia, foglio 132, Norcia. Roma: Regio Ufficio Geologico.](#)
- 1075 Schmid, S.M., Fügenschuh, B., Kissling, E. and Schuster, R., 2004. Tectonic map and overall architecture of the Alpine orogen. *Eclogae Geologicae Helveticae*, 97, pp.93-117.
- Schmid, S.M., Fügenschuh, B., Kounov, A., Matenco, L., Nievergelt, P., Oberhänsli, R., Pleuger, J., Schefer, S., Schuster, R., Tomljenović, B. and Ustaszewski, K., 2020. Tectonic units of the Alpine collision zone between Eastern Alps and western Turkey. *Gondwana Research*, 78, pp.308-374.
- Scholz, C.H., 2019. *The mechanics of earthquakes and faulting*. Cambridge university press.

- 1080 Scisciani, V., Esestime, P., 2017. The Triassic evaporites in the evolution of the Adriatic Basin. In: Soto, J.I., Flinch, J.F., Tari, G. (Eds.), *Permo-Triassic salt provinces of Europe, North Africa, and Atlantic margins: Tectonics and Hydrocarbon Potential*. Elsevier, Amsterdam, 499-516.
- Scognamiglio, L., Margheriti, L., Mele, F.M., Tinti, E., Bono, A., De Gori, P., Lauciani, V., Lucente, F.P., Mandiello, A.G., Marcocci, C. and Mazza, S., 2012. The 2012 Pianura Padana Emiliana seismic sequence: locations, moment tensors
1085 and magnitudes. *Annals Geophysics*.
- Sorlien, C.C., Seeber, L., Broderick, K.G., Luyendyk, B.P., Fisher, M.A., Sliter, R.W. and Normark, W.R., 2013. The Palos Verdes anticlinorium along the Los Angeles, California coast: Implications for underlying thrust faulting. *Geochemistry, Geophysics, Geosystems*, 14(6), pp.1866-1890.
- Stampfli, G.M. and Borel, G.D., 2002. A plate tectonic model for the Paleozoic and Mesozoic constrained by dynamic
1090 plate boundaries and restored synthetic oceanic isochrons. *Earth and Planetary science letters*, 196(1-2), pp.17-33.
- Sugan, M., Campanella, S., Chiaraluce, L., Michele, M., & Vuan, A., 2023. The unlocking process leading to the 2016 Central Italy seismic sequence. *Geophysical Research Letters*, 50, e2022GL101838. <https://doi.org/10.1029/2022GL101838> Received 21 OCT 2022 Accepted 12 JAN 2023 10.1029/2022GL101838.
- Takashimizu, Y., Kawakami, G. and Urabe, A., 2020. Tsunamis caused by offshore active faults and their deposits. *Earth-
1095 Science Reviews*, 211, p.103380.
- Tavernelli, E., 1997. Structural evolution of a foreland fold-and-thrust belt: the Umbria-Marche Apennines, Italy. *Journal of Structural Geology*, 19(3-4), pp.523-534.
- Tavernelli, E., Scisciani, V., Patruno, S., Calamita, F., Pace, P. and Iacopini, D., 2019. The role of structural inheritance in the evolution of fold-and-thrust belts: insights from the Umbria-Marche Apennines, Italy.
- 1100 Tertulliani, A., Arcoraci, L., Berardi, M., Bernardini, F., Brizuela, B., Castellano, C., Ercolani, E., Graziani, L., Maramai, A., Rossi, A. and Sbarra, M., 2012. The Emilia 2012 sequence: a macroseismic survey. *Annals of Geophysics*.
- Tinterri, R., Lipparini, L., 2013. Seismo-stratigraphic study of the Plio-Pleistocene foredeep deposits of the Central Adriatic Sea (Italy): geometry and characteristics of deep-water channels and sediment waves. *Mar. Petrol. Geol.*, 42, 30-49.
- Tizzani, P., Castaldo, R., Solaro, G., Pepe, S., Bonano, M., Casu, F., Manunta, M., Manzo, M., Pepe, A., Samsonov, S. and Lanari, R., 2013. New insights into the 2012 Emilia (Italy) seismic sequence through advanced numerical modeling of ground
1105 deformation InSAR measurements. *Geophysical research letters*, 40(10), pp.1971-1977.
- Tizzani, P., Castaldo, R., Solaro, G., Pepe, S., Bonano, M., Casu, F., Manunta, M., Manzo, M., Pepe, A., Samsonov, S. and Lanari, R., 2013. New insights into the 2012 Emilia (Italy) seismic sequence through advanced numerical modeling of ground deformation InSAR measurements. *Geophysical research letters*, 40(10), pp.1971-1977.
- 1110 Ustaszewski, K., Kounov, A., Schmid, S.M., Schaltegger, U., Krenn, E., Frank, W. and Fügenschuh, B., 2010. Evolution of the Adria-Europe plate boundary in the northern Dinarides: From continent-continent collision to back-arc extension. *Tectonics*, 29(6).

- van Unen, M., Matenco, L., Nader, F.H., Darnault, R., Mandic, O. and Demir, V., 2019. Kinematics of foreland-vergent crustal accretion: Inferences from the Dinarides evolution. *Tectonics*, 38(1), pp.49-76.
- 1115 Vannoli, P., Burrato, P. and Valensise, G., 2015. The seismotectonics of the Po Plain (northern Italy): Tectonic diversity in a blind faulting domain. *Pure and Applied Geophysics*, 172, pp.1105-1142.
- Wells, D.L. and Coppersmith, K.J., 1994. New empirical relationships among magnitude, rupture length, rupture width, rupture area, and surface displacement. *Bulletin of the seismological Society of America*, 84(4), pp.974-1002.
- Wrigley, R., Hodgson, N., Evestime, P., 2015. Petroleum geology and hydrocarbon potential of the Adriatic basin, offshore Croatia. *J. Petrol. Geol.* 38 (3), 301–316.
- 1120

Web references

<https://diss.ingv.it/>

<https://www.terremoti.ingv.it>

<https://www.videpi.com>

- 125 [United States Geological Survey \(USGS\). \(n.d.\). Earthquake magnitude, energy release, and shaking intensity. Retrieved from https://www.usgs.gov/programs/earthquake-hazards/earthquake-magnitude-energy-release-and-shaking-intensity.](https://www.usgs.gov/programs/earthquake-hazards/earthquake-magnitude-energy-release-and-shaking-intensity)

1130